Hindawi
Geofluids
Volume 2021, Article ID 8895350, 21 pages
https://doi.org/10.1155/2021/8895350

Research Article

Experimental Investigation on Organic Matter Orientation Characteristics of Terrestrial and Marine Shale in China

Dunqing Liu,[1,2] Hongkui Ge,[1,2] Yinhao Shen,[1,2] and Kui Zhang[3]

[1]*State Key Laboratory of Petroleum Resources and Prospecting, China University of Petroleum, Beijing 102249, China*
[2]*Unconventional Natural Gas Institute, China University of Petroleum, Beijing 102249, China*
[3]*CNPC Engineering Technology R&D Company Limited, Beijing 100007, China*

Correspondence should be addressed to Hongkui Ge; gehongkui@163.com

Received 10 April 2020; Revised 24 August 2020; Accepted 6 March 2021; Published 7 April 2021

Academic Editor: Constantinos Loupasakis

As an essential component in shale, OM (organic matter) grains and their arrangements may play essential roles in affecting the anisotropy of the reservoir. However, OM grains are commonly treated as an evenly distributed isotropic medium in current studies, and few works have been done to investigate their detailed arrangement characteristics. In this study, terrestrial and marine shale samples were collected from three different shale plays in China, and the arrangement characteristics of OM grains in each sample were investigated by SEM (scanning electron microscope) image analysis. The results indicate that OM grains in shale are not evenly distributed in isotropic medium, and their directional alignment is pervasive in both marine and terrestrial shale. OM grains in shale tend to subparallel to the bedding section, and their orientation degree and controlling factors differ among different shales. OM grains in samples from terrestrial C-7(Chang-7 Formation) exhibit the strongest directionality in their arrangement, and OM grains in samples from marine LMX (Longmaxi Formation) shale in the Fuling area also exhibit strong directional alignment. While in samples from marine LMX shale in the Baojing area, their directional alignment is much weaker. Shales with high clay content, high TOC (total organic carbon), low thermal maturity, and flat reservoir structure get more OM grains parallel to the bedding section. The biogenetic texture of graptolite in marine LMX shale is the dominating factor leading to the strong directional alignment of the OM grains. However, syncline structure may disorganize the preformed directional alignment and weaken the directionality of the OM grains, which results in the OM arrangement difference between LMX samples from Fuling and Baojing. While the compaction of the layered clay particles is the dominating mechanism leading to the strong directional alignment of the OM grains in terrestrial shale samples from C-7.

1. Introduction

Shales are multiphase, multiscale, and compositionally diverse sedimentary rock, and with the development of horizontal drilling and hydraulic fracturing technology in recent years, shale has become a research hotspot across the world [1, 2]. Besides their low porosity and ultralow permeability, shales also get more complex mineral composition than conventional reservoirs. Besides quartz, feldspar, and calcite, they also contain considerable amounts of clay minerals, and a few but nonnegligible OM is another essential component of shale [3]. The complexity in mineral constituent results in the complex pore structure and fickle mineral arrangement, and both factors endowed shale with much stronger anisotropy than conventional reservoirs [4, 5].

The manifestation of anisotropy in shale is diverse, among which elastic wave velocity, permeability, and mechanical properties are the most focused points from the field to the lab. These anisotropic characteristics play critical roles in the exploration and development of the shales, and scholars focus on this topic believe the anisotropy exhibited in shale is mainly attributed to the alignment of clay minerals, nonspherical pores, or microcracks [6, 7]. Their effects on gas transport, methane adsorption, fracture development, and other aspects have been widely investigated [8–11]. Among these studies, the alignment of clay minerals and

natural fractures is the most emphasized factors, and they were regarded as the major factors controlling the heterogeneity of shale [12–14]. Besides, several compositional and arrangement models have been presented to predict the petrophysical parameters of the shales [15, 16]. However, the arrangement of OM was not considered in these models.

Besides clay and fractures, many researchers have pointed out that certain OM particles are not evenly distributed in the shale matrix, and some OM particles may get an elongated shape and show specific directionality in their alignment [17, 18]. Nevertheless, detailed studies on OM grains orientation have seldom been carried out, and OM is still regarded as an evenly distributed isotropic medium in most of the models. The orientation of the OM grain was neglected in these models, and the corresponding excuse is their low content. However, the TOC in some shales with rich OM sources can reach 20% [19], and OM grains may take a very considerable volume due to their much lower density. Additionally, new nanocomputed tomography and SEM studies have revealed that OM grains with highly developed pores may form into continuous organic frameworks, and these OM grains with good connectivity may form a dominant pathway in shale. Thus, their arrangement may intensify the permeability anisotropy of shale [20]. Furthermore, studies also indicated that some types of OM grains without organic pores might still exhibit anisotropy in their inner structure due to their biogenetic texture [21], which may also affect the anisotropy of shale if they were directionally arranged.

Besides organic pores, studies have also shown that microfractures in shale are closely related to the elongated OM particles [22]. Recent nanoindentation and AFM (atomic force microscope) studies have proved that Young's modulus of the OM grains in shale is much lower than clay or other inorganic minerals and OM is the softest part in shale [23–25], and the development of organic pores may further lower their Young's modulus [26]. Besides, OM grains also get a much larger thermal expansivity than the ambient inorganic mineral particles [27]. These features make OM grains in shale more sensitive to the stress and thermal change during deposition, compaction, and thermal maturation. Thus, fractures are more likely to be formed at the boundary between OM and inorganic mineral particles, which may further affect the anisotropy on permeability, elastic wave velocity, and other vital features in return. Thus, the orientation of OM grains in shale deserves more attention and investigation.

In this study, marine and terrestrial shale samples were collected from 4 wells in China, and their mineral constituent, TOC, and Ro were investigated. The morphological and arrangement characteristics of OM grains in each sample were compared and investigated by SEM image processing. Moreover, the effects of mineral contents, TOC, and thermal maturity on OM grain orientation and the corresponding forming mechanism were also discussed.

2. Samples and Methods

The detailed parameters of the shale samples used herein are listed in Table 1. The mineralogical composition was obtained by XRD (X-ray diffractometer) (model Bruker D8, 45kv, 35 mA) at State Key Laboratory of Petroleum Resources and Prospecting at China University of petroleum, Beijing. The analysis was performed in accordance with Chinese Oil and Gas Industry Standard SY/T 5163-2010. The TOC of samples JY11 and JY45 was obtained by a carbon and sulfur analyzer (model LECO CS844) in the test center of Exploration and Development Institute in Jianghan Oil Field, Wuhan, and the analysis was performed in accordance with Chinese National Standard GB/T 19145-2003. The TOC of the rest two samples and R_o data were acquired from relevant literature.

Sample JY11 and JY45 were collected from Fuling shale gas play in Chongqing, which is the largest shale gas play in China. Sample BY was collected from an exploratory well in the Baojing area, Hunan. These three samples were all collected from LMX, which is characterized by high OM abundance and favorable organic types to generate large amounts of gas. Sampled JY11 and JY45 were collected from the same submember of LMX, and their TOC, R_o, and mineral constituent are very similar. Their TOC is around 3%, and their R_o ranges from 1.8% to 2.9%, suggesting a stage of high maturity and more complicated diagenesis. While the R_o of sample BY is 3.28%, which is the highest among the four samples. Sample YY was collected from C-7, Shanxi, which is a typical terrestrial shale. The TOC of the samples from C-7 ranges from 1.7% to 9.8%, with a mean value of 5.73%. The R_o of samples from C-7 is much lower than LMX, which ranges from 0.7% to 1.3%, indicating sample YY is within the oil window stage.

According to the XRD results, siliceous and clay minerals are the dominating minerals in the four samples. Sample YY has the highest clay content, which is over 50%, and quartz occupied another 25.1%. While in sample JY11, JY45, and sample BY, the clay content is around 30% and quartz occupied about 40%. The specific types of clay minerals in these samples were not further analyzed. According to the researches of Yang et al. [28] and Ji et al. [31], the predominant clay mineral in LMX shale is illite, which accounts for more than 65%, and the primary clay mineral in terrestrial C-7 shales is illite-smectite mixed layers (with an average value of 43%) and then followed by illite ranging from 25% to 48%.

During the sample preparation, abundant graptolites were found on samples collected from LMX, and their amount is much larger in samples from Fuling than that in samples from Baojing. Researches have indicated that graptolites in shale can contribute to TOC [32, 33], and as Figure 1(a) shown, these graptolites are usually subparallel to the bedding section. Thus, it may be an important part of contributing to the directionality of the OM grains in shale. As shown in Figure 1(b), small shale pieces were collected to investigate the mineral constituent and detailed microstructure of the graptolites. A field emission SEM (model FEI quanta200) was adopted to capture SEM images of the graptolites. These small samples were not polished to keep their microstructure, and they were all coated with a thin gold film to enhance the image quality.

Besides these small samples, slice samples were also prepared to investigate the OM orientation. As shown in

Table 1: Parameters of the shale samples.

Sample	Formation	Sedimentary Environment	Source	TOC (wt%)	R_o (%)	Mineralogical composition (wt%)				
						Clay	Quartz	Feldspar	Calcite	Pyrite
JY11	LMX	Marine	Jaoshiba	3.3	1.8-2.9[a]	28.9	47.1	8.8	10.8	4.4
JY45	LMX	Marine	Jaoshiba	3.03	1.8-2.9[a]	32.2	39.5	8.3	15.7	4.3
BY	LMX	Marine	Baojing	2.33[b]	3.28[b]	27.5	44.9	12.2	11.3	4.1
YY	C-7	Terrestrial	Yanchang	1.7-9.8[c]	0.7–1.3[a,c]	50.3	25.1	2.2	17.2	5.2

Note: [a]The data was from [28]. [b]The data was from [29]. [c]The data was from [30].

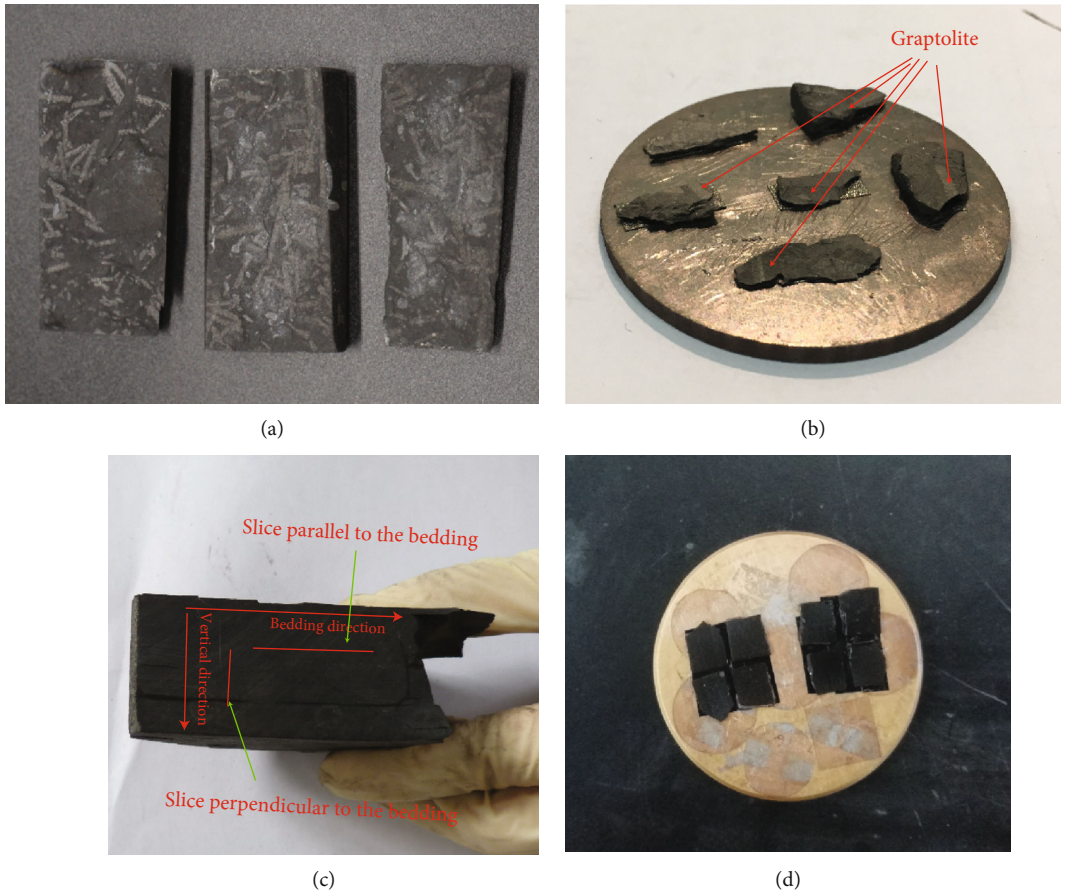

Figure 1: Shale samples used in this study. (a) Samples with abundant graptolites. (b) Samples for graptolite observation. (c) Schematic plot of the cutting direction. (d) Slice samples after polishing and coating.

Figure 1(c), two slices were orthogonally cut out from each sample, among which one sample is parallel to the bedding section and the other is vertical to the bedding section. For the convenience of the expression in the rest of this paper, we call the profile parallel to bedding direction as TS (transverse section), and the profile vertical to bedding direction as LS (longitudinal section). The slice samples were firstly mechanically polished and then polished by argon-ion to enhance surface flatness. Moreover, all these slice samples were coated with a thin gold film to enhance the image quality. Slice samples complete coating and polishing are shown in Figure 1(d), and a cold field emission SEM (model Hitachi SU8010) was adopted to capture images from these slice samples.

According to our tests, SEM images captured at ×500 or ×1000 magnification can reach the right balance between ideal OM grain quantity and acceptable sharpness, and both factors are critical to the accuracy of the subsequent image processing and analysis. The SEM image capturing was conducted in the State Key Laboratory of Petroleum Resources and Prospecting at China University of Petroleum, Beijing. As SEM images herein were saved as 8 bits grayscale figures, the brightness of the particles is in direct proportion to the atomic number of the elements inside. Thus, OM grains in SEM images usually are much darker than the ambient inorganic minerals, and pyrite grains usually are the brightest [34]. Based on that brightness contrast, the Weka Trainable Segmentation plugin in Image J segmented the OM grains

and pyrite grains in all SEM figures. This plugin is a machine learning-based semiautomatic tool to produce pixel-based segmentations, and it has been widely used as a powerful and efficient tool in SEM image processing [35].

Figure 2 demonstrates the image processing steps. After the OM and pyrite segmentation, they were identified and numbered by Analyze Particles Function in Image J. This function can find the major axis and minor axis of the identified particle, and the AR (aspect ratio) as well as the angle between the major axis and horizontal axis was then calculated. The AR can reflect the shape of the grains, and the angle represents their orientation. Particles with an area smaller than 20 pixel^2 (the resolution of the SEM image is 1280×960) were excluded to reduce the influence of pixel noises. The segmented OM and pyrite grains were then merged into one figure to investigate their coexistence relationship. 7 to 9 images were captured from each slice sample, and the statistical data of MA (mean angle) and SDA (standard deviation of the angles) of each image were then calculated. The MA indicates the central tendency of the grain orientation, and the SDA indicates the dispersion degree of the grain orientation. Sample with smaller SDA means OM grains inside get more definite directionality in their orientation, and there are more OM grains parallel to the MA direction.

3. Results

3.1. Characteristics of the Graptolite under SEM. Graptolites are widely distributed in organic-rich LMX shale in South China, and it has been reported to be closely related to the OM enrichment in LMX shale [36, 37]. According to the core observation, most graptolites are preserved as black or gray lamellate films, and their distribution can be clump together or randomly dispersed. Due to the overlap effect, the size of the graptolite in core scale can reach several centimeters, and their abundance varies a lot from one core to another.

The chemical composition of graptolite is controversial, and the chitinous substance was initially believed to be the main composition. Subsequent studies demonstrated that aromatic structure with aliphatic groups consisted of the main body of graptolite. Thus, it will dealkylate during the maturation and can act as good hydrocarbon-generating material in shale [38]. The EDS results shown in Figure 3 indicate that carbon is the dominant element of the graptolite in our samples, and several related studies have also drawn similar conclusions [39, 40]. Due to its unique biogenetic texture, the geometrical characteristic of graptolite may differ significantly from other OM grains.

As shown in Figure 4(a), the graptolite (indicated by the yellow dash line) is in a lamellar structure with a width of several millimeters, while the length can reach several centimeters. The main body of graptolite is made up of cortex and central canal (Figure 4(b)), and the size of these lamellar cortexes is around dozens of microns, which is much larger than the ambient inorganic grains. Moreover, a sharp boundary can be observed between the lamellar cortex and the outside matrix (Figures 4(b) and 4(c)).

Unlike most OM grains in shale that developed with massive spongy pores, only a few shallow pores can be observed on these lamellar cortexes (Figure 4(c)). Some lamellar cortex has broken into several fragments, suggesting lamellar cortex may be more brittle than those amorphous OM grains (Figure 4(d)), and the surface of these lamellar cortexes is much smoother than other grains in the matrix, which may reduce its adhesive strength with the ambient mineral particles. Besides the shallow holes, a few moldic pores were found on the graptolite surface (Figure 4(e)), and the diameter of which can reach 2.5 μm. Organic pores in amorphous OM grains are usually under micron scale, while nanoscale organic pores were not observed in graptolites collected from Fuling samples. The absence of the nanoscale organic pores may cause by the shielding of the gold film, or it may be the result of low thermal maturity. In other studies, abundant nanometer-sized spongy pores were observed on the graptolites from LMX (Figures 4(g)–4(i)), and these spongy pores exhibited anisotropy inner the lamellar cortex. Moreover, most elongated organic pores were subparallel to the bedding section [36, 37]. The difference of the organic pore development in the graptolites indicates that the maturity of the graptolites may vary significantly among different shale plays.

The maturity of graptolite is not easy to be identified from SEM images, but the color of graptolites with lower thermal maturity is usually much darker [33]. Moreover, spongy pores are more developed in OM particles with higher thermal maturities. These features can help estimate the maturity of the OM grains. The color of the graptolites in our sample is dark black, and pores inner graptolites are less developed, both of which suggest the thermal maturity of the graptolite in LMX samples herein may be much lower than those amorphous OM grains. According to the SEM images, due to the biogenetic texture, these graptolites derived OM grains with lower thermal maturity may exhibit much stronger anisotropy in its structure and orientation.

3.2. Distribution Characteristics of the OM Particles

3.2.1. OM Orientation in Sample BY. As shown in Figures 5(a) and 5(b), most OM particles in sample BY are amorphous and they are dispersed randomly in both LS and TS, and the occurrence relationship between OM and pyrite particles is also irregular in both LS and TS. Pyrite grains in shale are usually coexisted with the OM particles [28], but the later OM maturation and diagenesis may alter their coexistence relationship. The OM particles in sample BY are not closely adjoined to those pyrite grains, suggesting sample BY may undergo intricate diagenetic processes, and these pyrite or OM grains may have migrated away from its original position.

Unlike graptolite-derived OM shown in Figure 3, the shape of most OM grains in sample BY is flocculent. According to the research of Curtis et al. [41] and Nie et al. [42], these flocculent or amorphous OM grains usually get higher maturity as the maturation may increase the inner pressure and induce more spongy pores. Those organic pores may destroy the structural integrity of the OM grains, and the

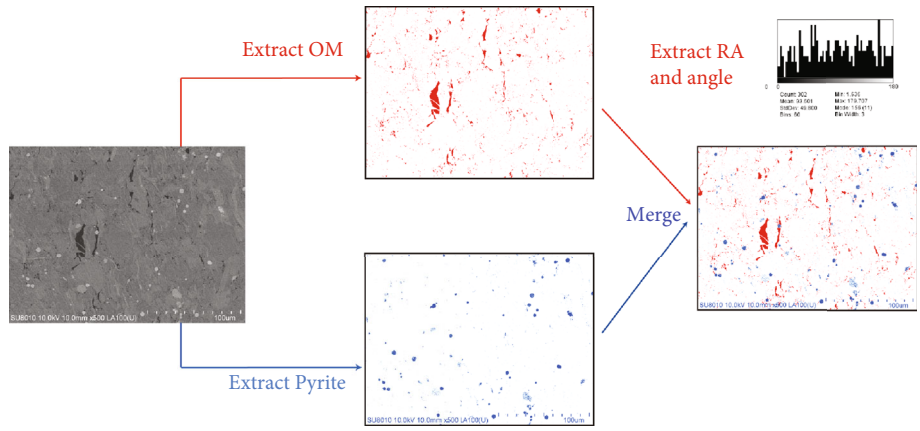

Figure 2: Typical image processing procedures.

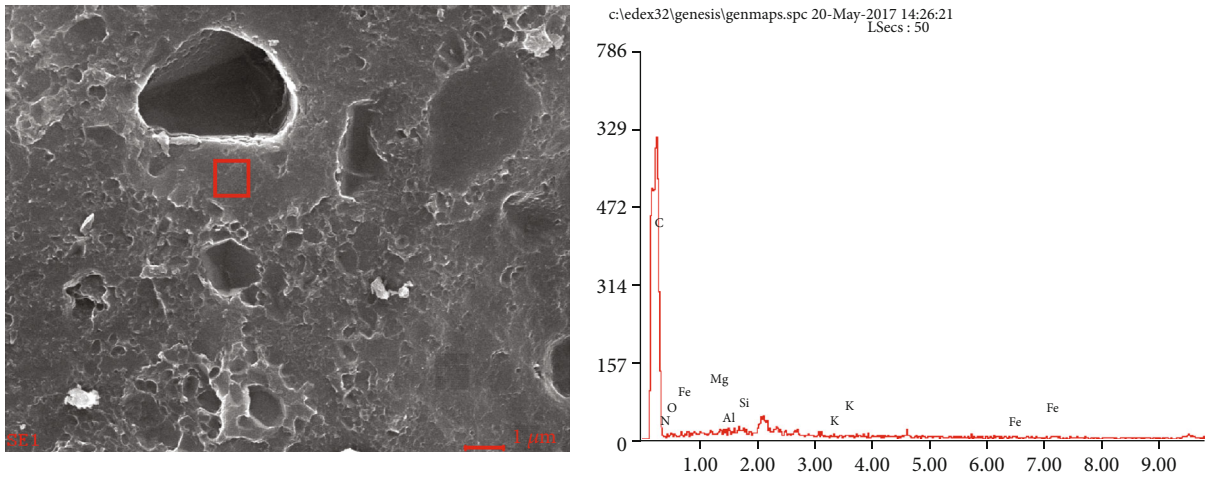

(a) (b)

CK	89.09	91.17
NK	06.38	05.60
OK	03.80	02.92
MgK	00.16	00.08
AlK	00.22	00.10
SiK	00.24	00.10
KK	00.00	00.00
FeK	00.11	00.02
Matrix	Correction	ZAF

(c)

Figure 3: EDS (energy dispersive spectrometer) spectrums and elements content of graptolite. (a) The red box indicates the area where the element was analyzed. (b) The spectrum of the EDS. (c) Elements content results.

increasing inner pressure may push OM into other intergranular pores or fractures. Moreover, subsequent sedimentation and compaction may intensify the distortion of the OM grains.

Besides these flocculent OM particles, a few banded OM grains were also observed in LS (indicated by dash boxes in Figure 5(a) (vi, vii, viii)), which get sharp edges and elongate structure. It is quite easy to identify graptolites in cores or outcrop due to their biological structures, but it is challenging to identify them under ×500 or ×1000 magnification because their biological structure was weakened by the cutting and polishing processes. In contrast to those flocculent OM particles, graptolite remains get much larger AR and most of them are subparallel to TS. Considering the geometrical feature of those OM grains and the morphology study of Luo et al. [33], we believe those banded OM grains in sample BY are highly

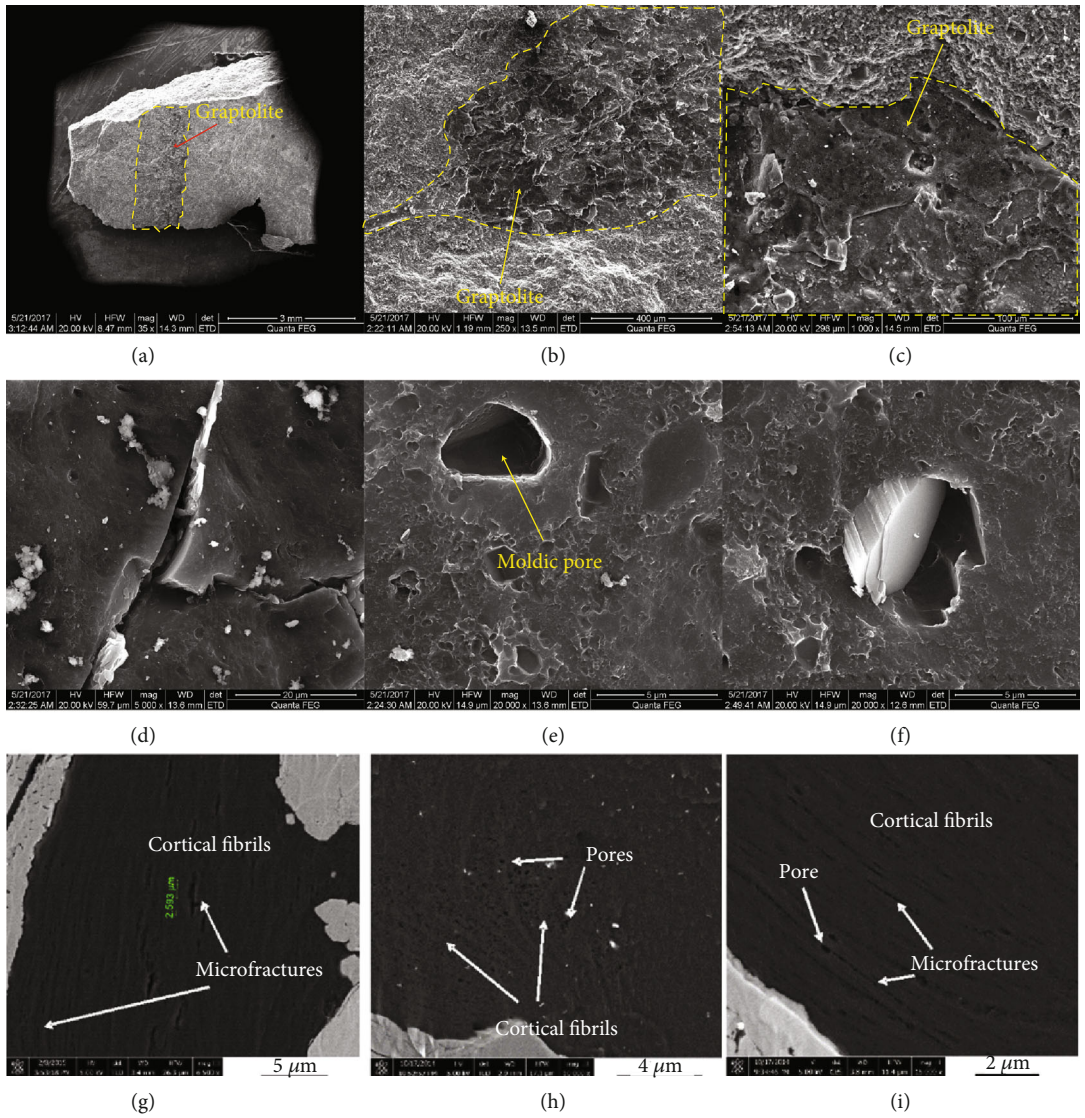

Figure 4: Microstructure of the graptolite under SEM. (g)–(i) are modified from [36].

likely to be graptolite remains, and they may contribute more to the anisotropy than these amorphous OM grains due to their more directed orientation and much larger AR. However, their overall contribution to the anisotropy may be limited by their quantity shortage.

As Figure 5(b) shows, OM gains are filled inner the intergranular pores of the pyrite grains (indicated by red dash line boxes) in LS, and the size of these pyrite grains is much larger than those without OM. The distribution of the OM grains in TS is more agminated than LS, and very few banded OM grains are observed in TS. Moreover, the orientation of these banded OM grains is more random in TS, while the distribution of pyrite grains is more inhomogeneous in both LS and TS, and their size in TS is slightly larger than the ones in LS. Due to the FOV (field of view) limitation, these inhomogeneous exhibited in grain size and distribution in sample BY are limited under the submillimeter scale. Besides those bonded OM grains in LS, most OM grains in sample BY exhibit weak directionality in their orientation in both LS and TS.

As shown in Figures 5(c) and 5(d), though it is unobvious in SEM images, the image processing results indicate that OM grains in LS of sample BY still show specific directionality, while the trend is much weaker in TS. The statistical results indicate that the average MA of the OM grains in LS is 95.07°, and the average SDA is 45.39°, while in TS, the average MA is 89.25°, and the average SDA is 53.02°. The average SDA indicates that the directionality of OM grains in LS is much stronger than TS in sample BY.

3.2.2. OM Orientation in Sample YY. Sample YY is a typical terrestrial shale, as shown in Figure 6(a), the structure of OM grains in sample YY differs quite a lot from sample BY. Due to its much higher TOC, the area and size of the OM grains in sample YY are much larger than that in sample BY, and most OM particles in sample YY are banded grains with lengths larger than several hundred of microns. The position of the pyrite grains in sample YY is much closer to OM grains than that in sample BY, and some pyrite grains (indicated by the black dash line boxes in Figure 5(a)) also

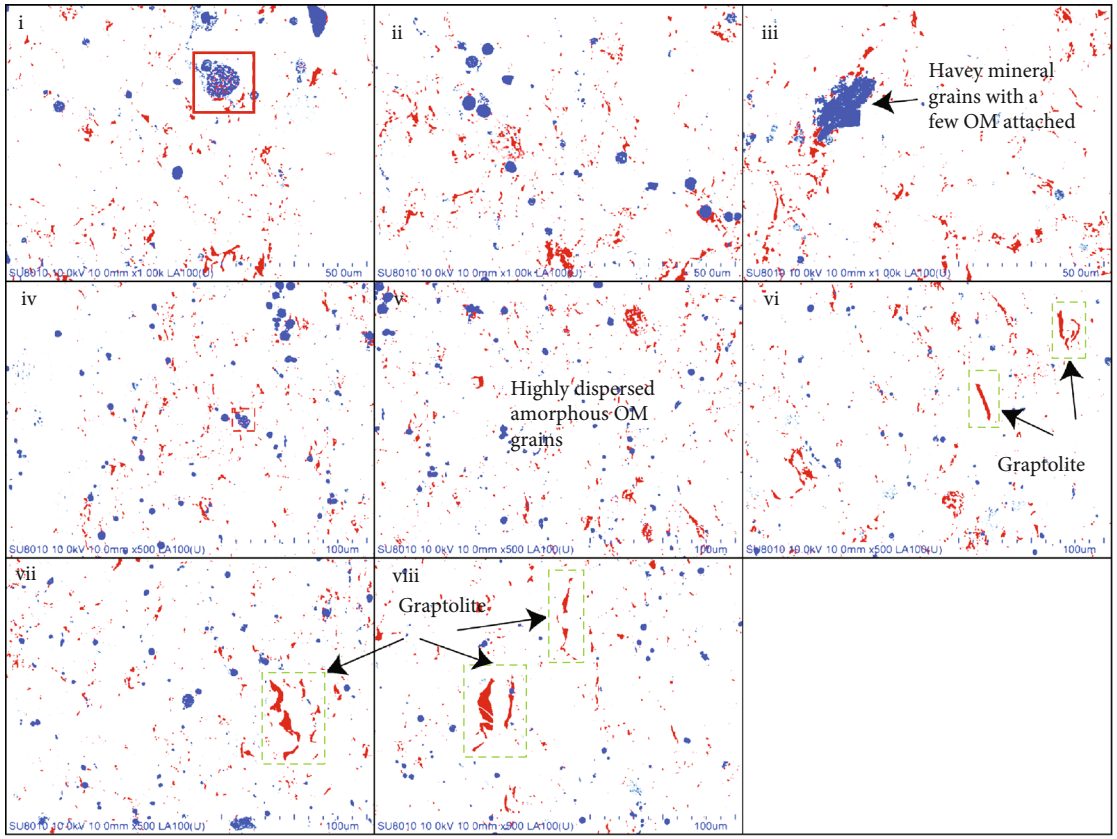

(a)

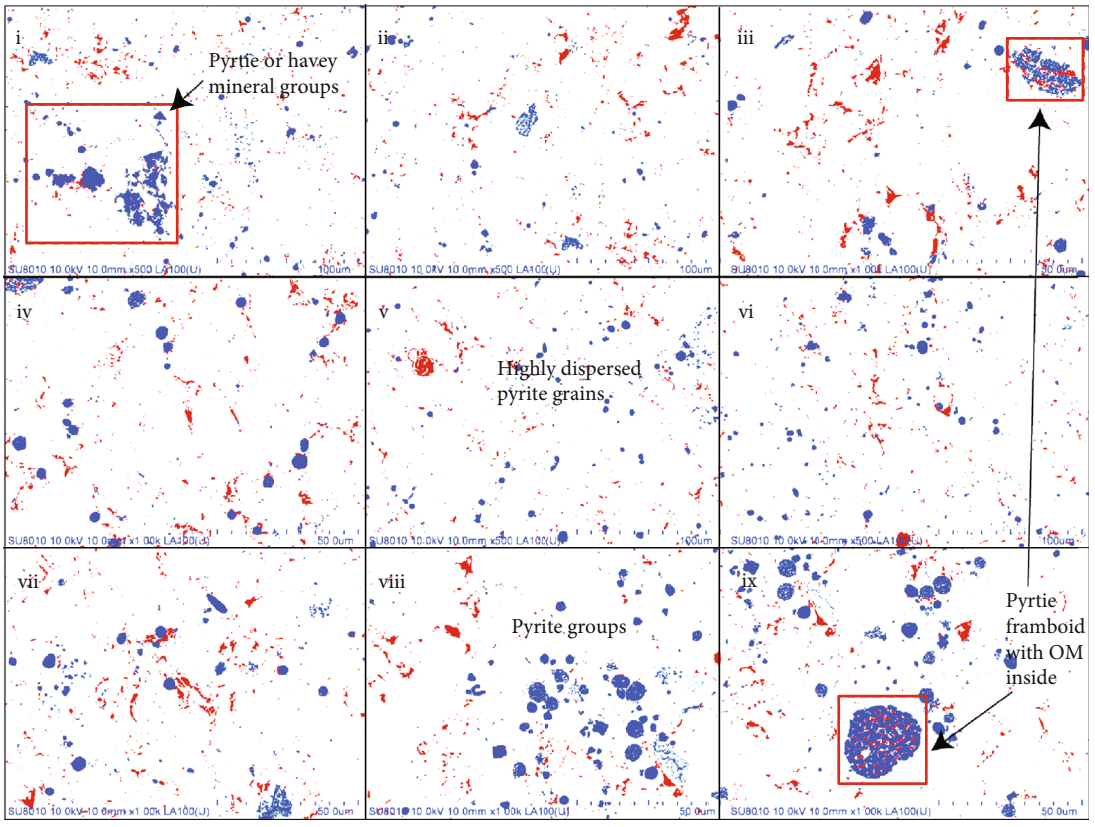

(b)

Figure 5: Continued.

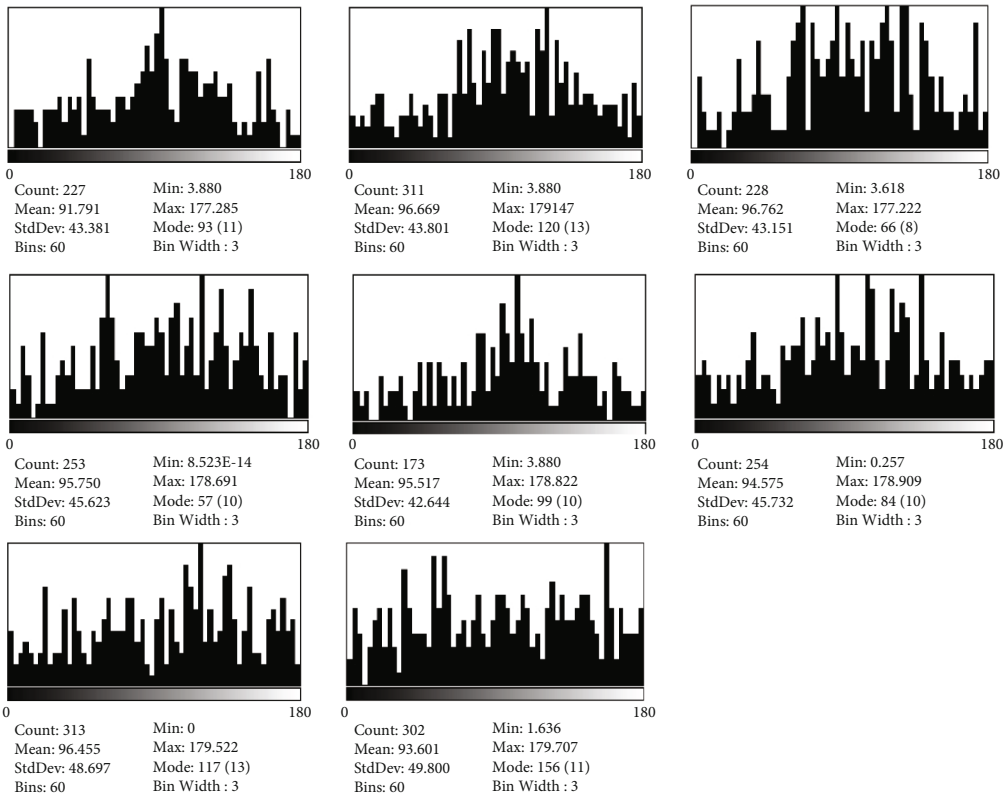

(c)

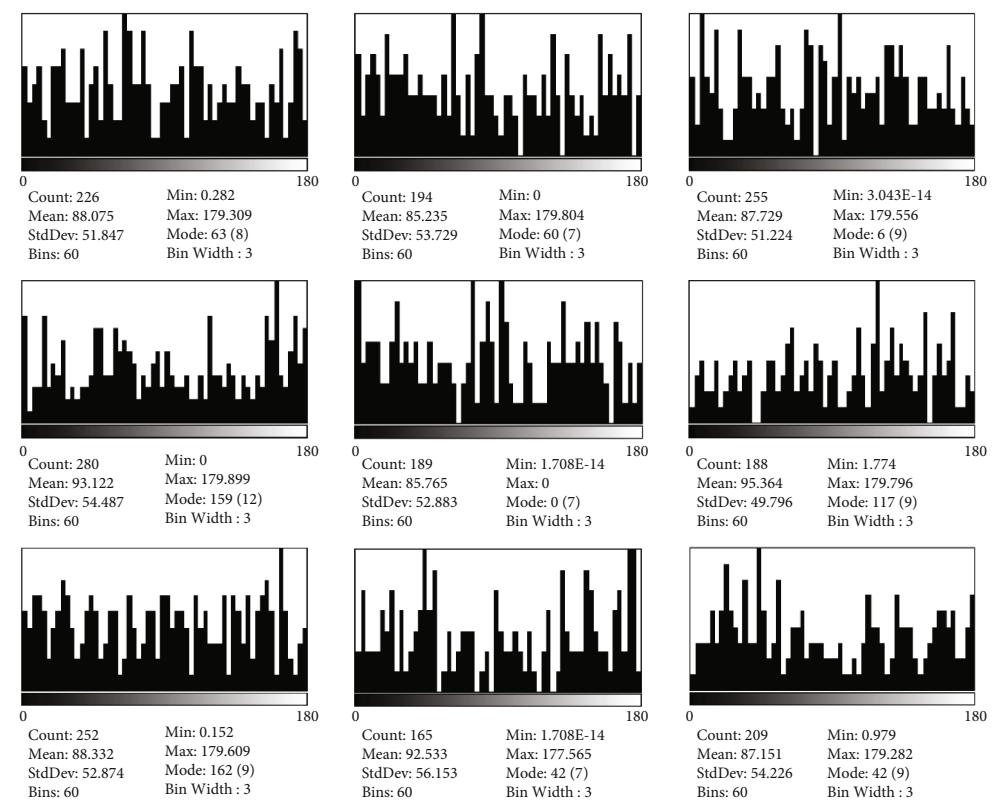

(d)

Figure 5: Images of sample BY after segmentation. The red part is OM, and the blue part is pyrite. (a) and (b) Merged images of sample BY in LS and TS. (c) and (d) The long axis angle distribution of the OM grains in LS and TS.

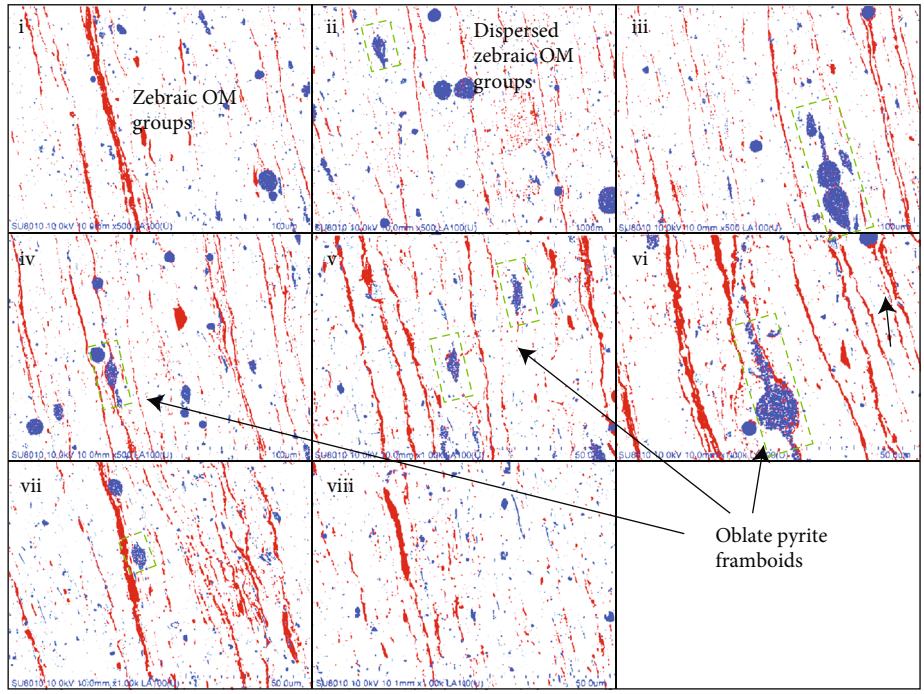

(a)

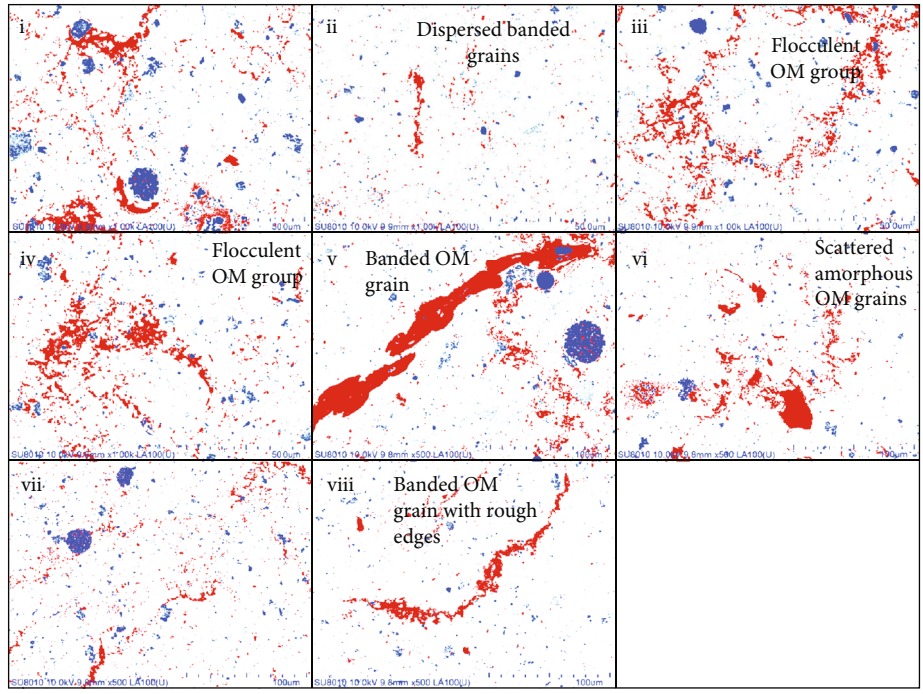

(b)

Figure 6: Continued.

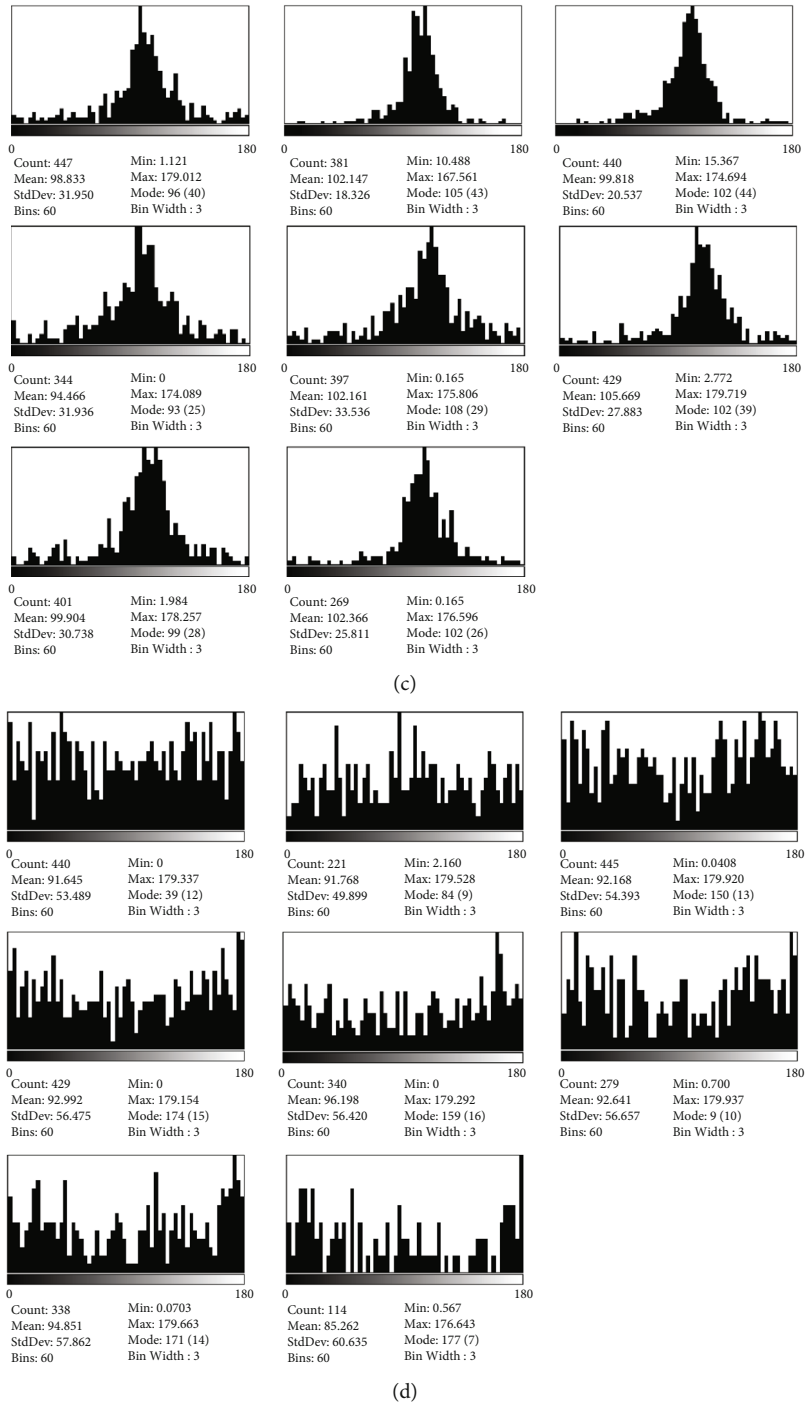

Figure 6: Images of sample YY after segmentation. The red part is OM, and the blue part is pyrite. (a) and (b) Merged images of sample BY in LS and TS. (c) and (d) The long axis angle distribution of the OM grains in LS and TS.

get banded shape. The directionality of the OM and pyrite particles in LS is much stronger and more evident than that in sample BY, and most OM and pyrite particles are subparallel to the bedding section. The boundaries of the banded OM grains in sample YY are not as smooth and clear as the ones in sample BY, but these OM particles contain very few inorganic mineral grains and get a more intact structure. As shown in Figures 6(c) and 6(d), the long axis angle distribution of the OM grains in sample YY is far more concentrated in LS, and the peak positions are almost the same. According to the statistical analysis, the average MA of the OM grains is 100.67°, and the average SDA is 27.59° in LS, which is much smaller than that in sample BY, indicating that OM grains in the LS of sample YY are strictly directionally orientated.

Though OM grains quantity is smaller in LS of sample YY, their size is much larger than that of sample BY. Banded OM grains were also observed in TS of sample YY, but they are much thicker than the ones in the LS. There are very

few amorphous OM grains in LS, but it can be widely observed in TS of sample YY, and its morphology shows certain differences with the ones in sample BY. The amorphous OM grains in sample BY get irregular edges and relatively intact inner structure, while in sample YY they get similar snatchy edges but contain more inner pores. Besides, the size of the amorphous OM grains in sample YY is much larger than the ones in sample BY. These differences indicate that mechanisms forming the amorphous OM grains in two samples may be different. Nevertheless, as Figure 6(d) shows, these OM grains in the TS of sample YY also exhibit no directionality as the ones in sample BY. The average MA is 92.19° and the average SDA is 55.73°, which is similar to that of sample BY.

3.2.3. OM Orientation in Sample JY45. Sample JY45 was collected from the largest gas shale play in China, and beddings are highly developed in the main production layer. As Figure 7(a)(i), (ii), (vii) shown, the banded OM grains are of the largest size among the four samples, but many inorganic grains are firmly attached or embedded in these the banded OM. As Figure 7(a) (iv), (v), (vi) shown, amorphous OM grains are also widely distributed in the TS of sample JY45, and their morphological characteristics are similar with ones in sample BY.

These banded OM grains in sample JY45 are highly likely to be graptolite remains cause their thickness is over dozens of microns, and the embedded inorganic grains may from the overlap of graptolite layers. These graptolites, as we observed from the core samples, are tabular organic films with centimeter-scale. They are well parallel to the bedding direction on the core scale, and their directionality is still distinct in these micron-scale SEM images. The quantity of the banded OM grains in LS of sample JY45 is much smaller than sample YY, but they also exhibit specific directionality in their orientation. However, due to their less intact structure, these banded OM grains may be identified as several smaller independent particles by the software, and, thus, the holistic orientation of the banded grains may be weakened in the image analysis results. According to which, the average MA and average SDA of the amorphous OM grains are 90.66° and 49.2° in LS, respectively. While SDA of the bonded OM grains ranges from 45°to 46°, both of which are much larger than sample YY.

While in TS, the distribution of OM grains in sample JY45 is as dispersed as sample BY. The size of the OM grains is much smaller than LS, and only a few annular OM grains can be observed (Figure 7(b) (i, ii, iii)). The number of pyrite grains in TS of sample JY45 is much smaller than sample BY, and the distribution of amorphous OM in sample JY45 is relatively wider than sample BY, and their structure is also more complicated. According to the image analyses shown in Figures 7(c) and 7(d), the average MA of the OM grains in TS is 87.89°, and the average SDA is 54.67°. Which is much larger than the LS, but it is almost the same with that in sample BY.

3.2.4. OM Orientation in Sample JY11. Sample JY11 was collected from the same shale play with sample JY45, and they are from the same sub-member of the major pay zone. However, the morphology of the OM grains in sample JY11 exhibits noticeable differences from sample JY45. As Figure 8(a) shows, the banded OM grains in sample JY11 are much thinner, and some are of rich branches (Figure 8(a) (i, ii, viii)). These ramifications may derive from the compressed graptolite multilayers, and some OM grains also involved many inorganic particles, but their overall structural integrity is much better than the banded ones in sample JY45. The distribution of pyrite grains in sample JY11 is also dispersive.

As Figure 8(c) shows, the angle distribution of the OM grains in sample JY11 is more centralized than sample JY45, and most peaks are located around 90°, suggesting the OM grains in the LS of sample JY11 tend to subparallel to the bedding direction. According to the image analysis, the average MA of the OM grains in sample JY11 is 94.5° in LS, and the average SDA is 41.93°, which is smaller than that of sample JY45 and sample BY, but much larger than sample YY, and the result agree well with the intuitive observation of the SEM images.

While in TS, the amount of the OM grain is the smallest and their distribution is also highly dispersed, and almost no banded OM grains were observed. The MA and SDA of the OM grains in sample JY11 are 94.5° and 54.29° in TS, indicating that the directionality of the OM grains in sample JY11 is much weaker in TS. The position of the pyrite grains in sample JY11 shows no significant correlation with the OM particles, especially in TS. While in sample JY45, more pyrite grains are involved with the OM grains.

4. Discussion

4.1. The Representativeness of SEM Images. The magnification used in this study was fixed to ×500 and ×1000 to ensure SEM images contain enough target particles and with acceptable sharpness as well. However, if the magnification is too large, the FOV will be too small to represent the characteristics of the sample. To estimate the representativeness of the SEM images, we calculated the area ratio of OM and pyrite grains in each image. As shown in Figure 9(a), the area ratio of OM grains in both LS and TS of the four samples exhibits a well positive correlation with the TOC data. While the consistency between pyrite area ratio and pyrite content calculated from XRD is weaker (Figure 9(b)), which may cause by the misidentification of Ca or Ba, as particles contain Ca or Ba in shale get similar brightness with pyrite, thus, they may be misidentified as pyrites. Nevertheless, the identification of OM is more precise cause OM grains get more evident differences in their density and composition. The TOC and XRD data of the four samples are derived from experiments according to relevant industry standards, and these results can accurately indicate the amount of the OM and pyrite in each sample. Thus, the positive correlation between XRD, TOC, and area percentage can prove the SEM images used herein can represent the difference of the OM grains in the four samples.

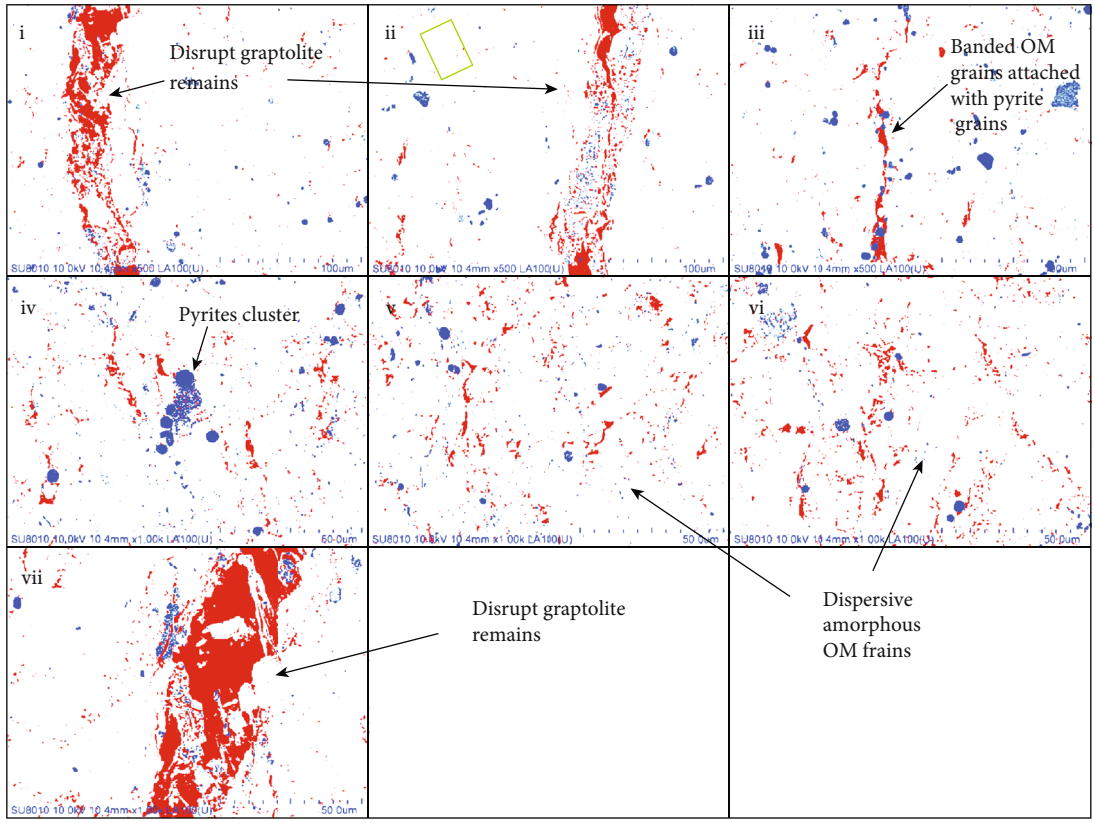

(a)

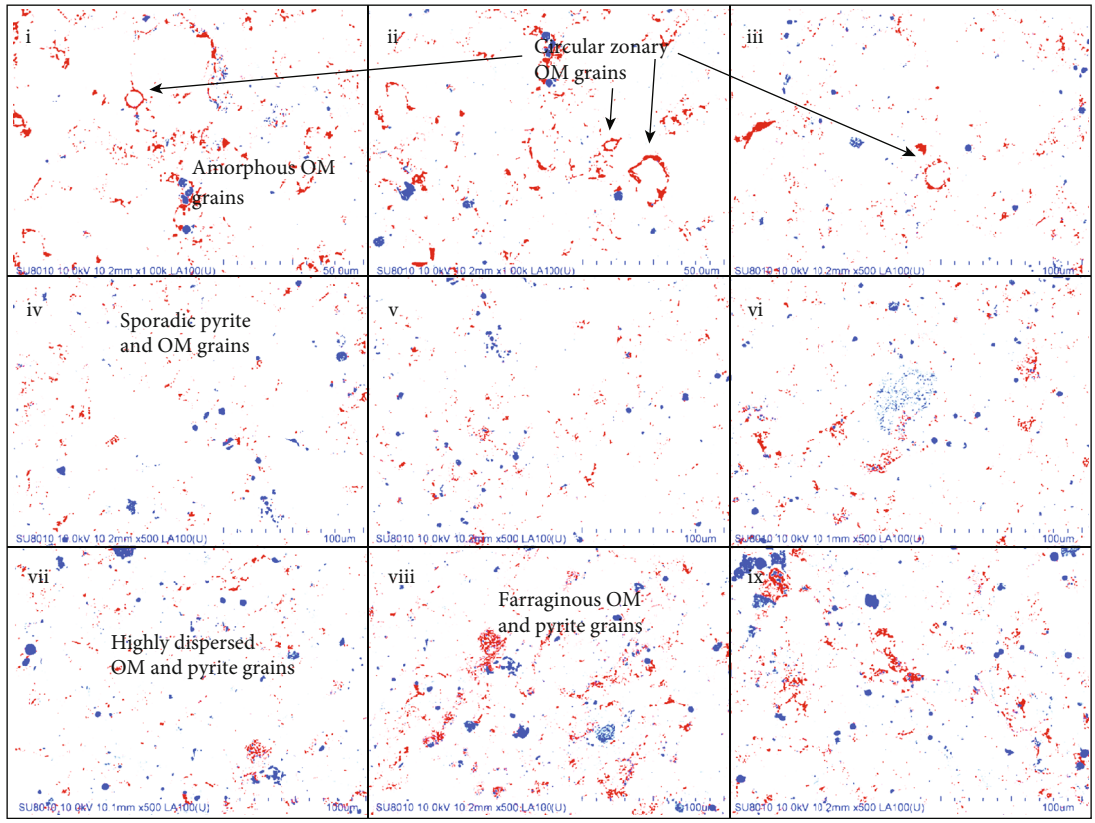

(b)

Figure 7: Continued.

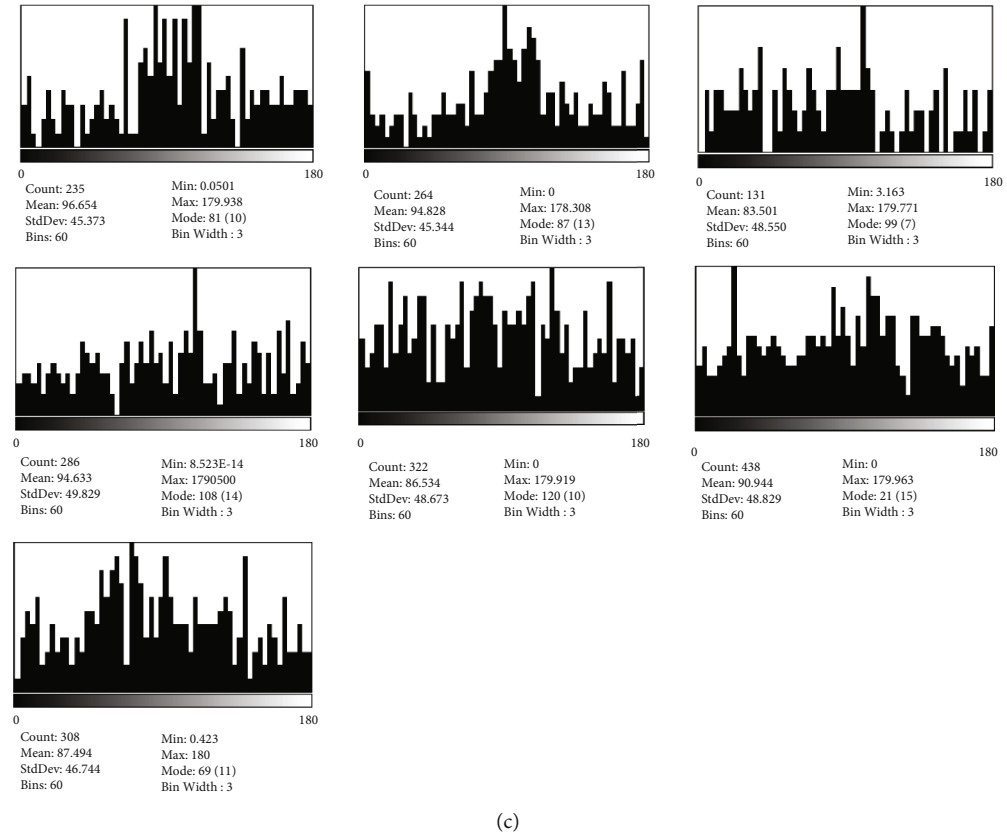

(c)

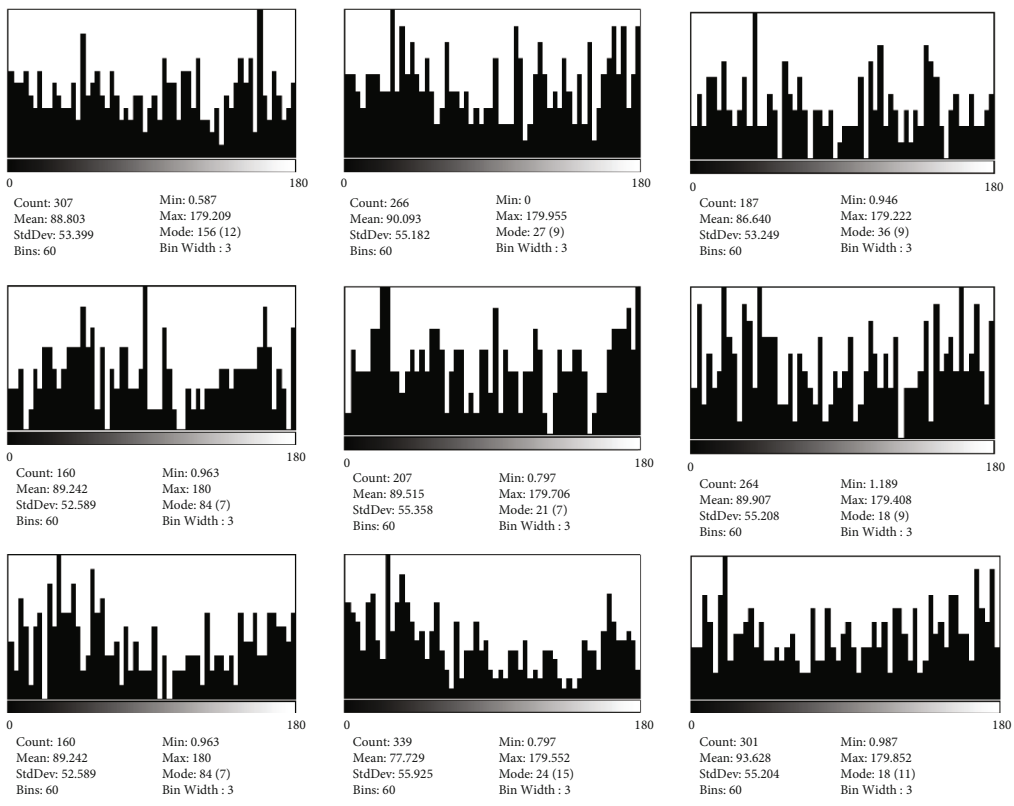

(d)

Figure 7: Images of sample JY45 after segmentation. The red part is OM, and the blue part is pyrite. (a) and (b) Merged images of sample BY in LS and TS. (c) and (d) The long axis angle distribution of the OM grains in LS and TS.

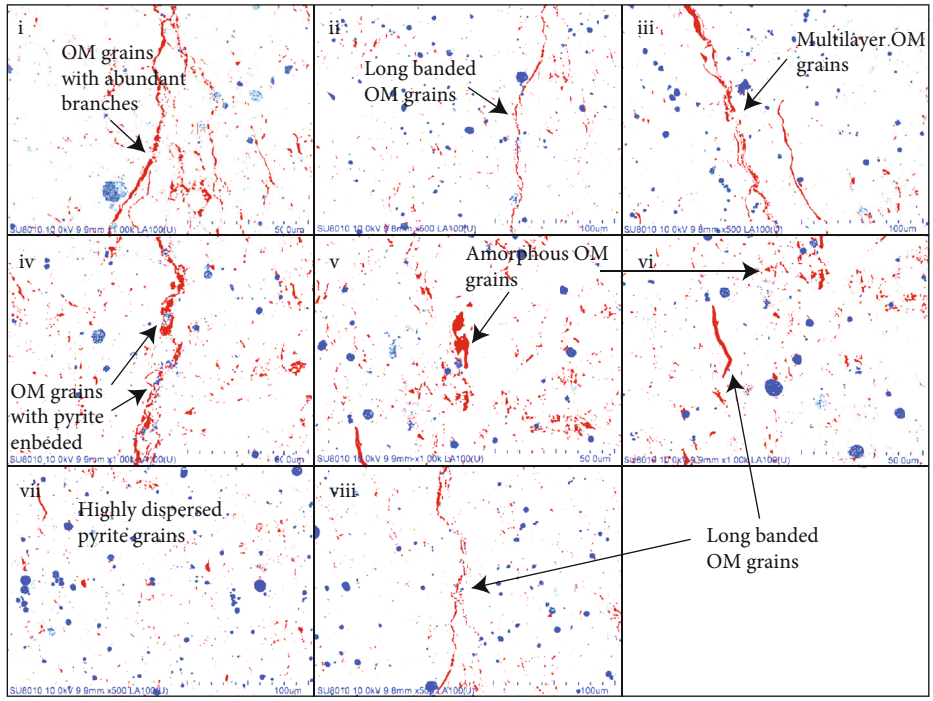

(a)

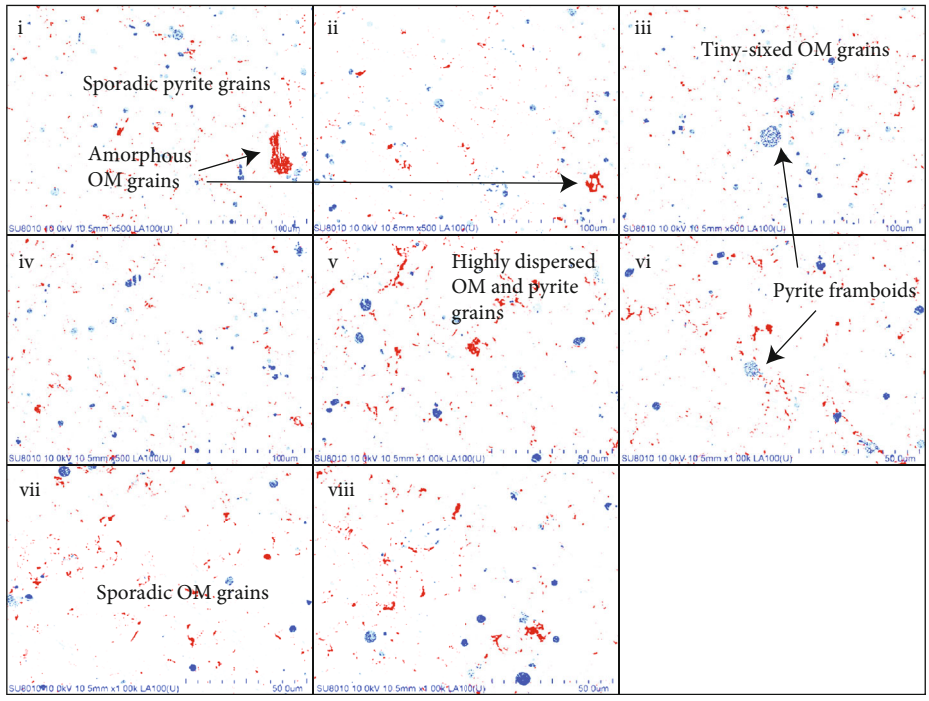

(b)

Figure 8: Continued.

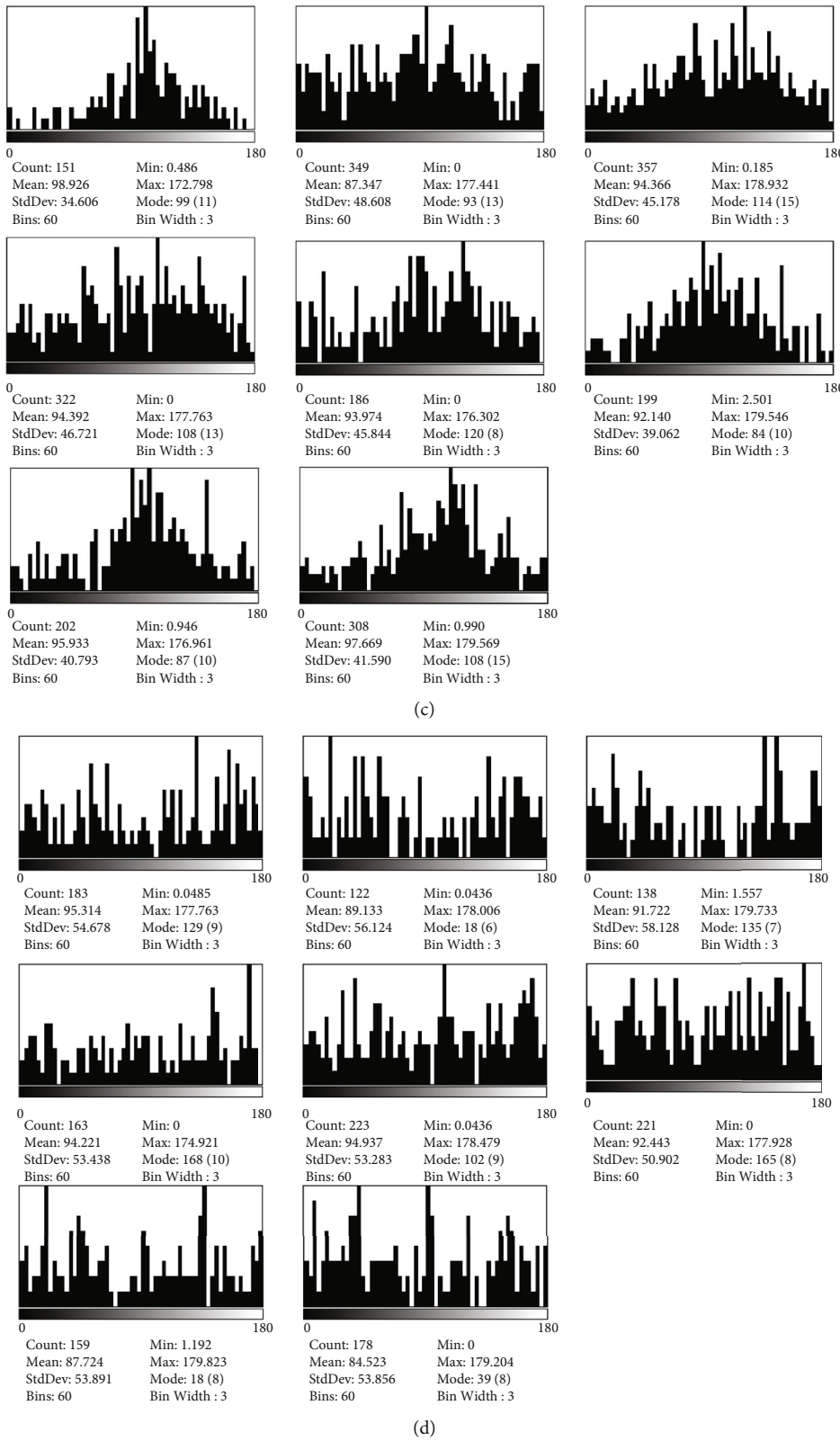

Figure 8: Images of sample JY11 after segmentation. The red part is OM, and the blue part is pyrite. (a) and (b) Merged images of sample BY in LS and TS. (c) and (d) The long axis angle distribution of the OM grains in LS and TS.

4.2. The Directional Characteristics of the OM Grains. As shown in Figure 10(a), the MA of the OM grains in both LS and TS of the four samples ranges between 85° to 95°, indicating the general tendency of the OM orientation in four samples is similar, all of which are subparallel to the bedding section and it may be a universal phenomenon in shale.

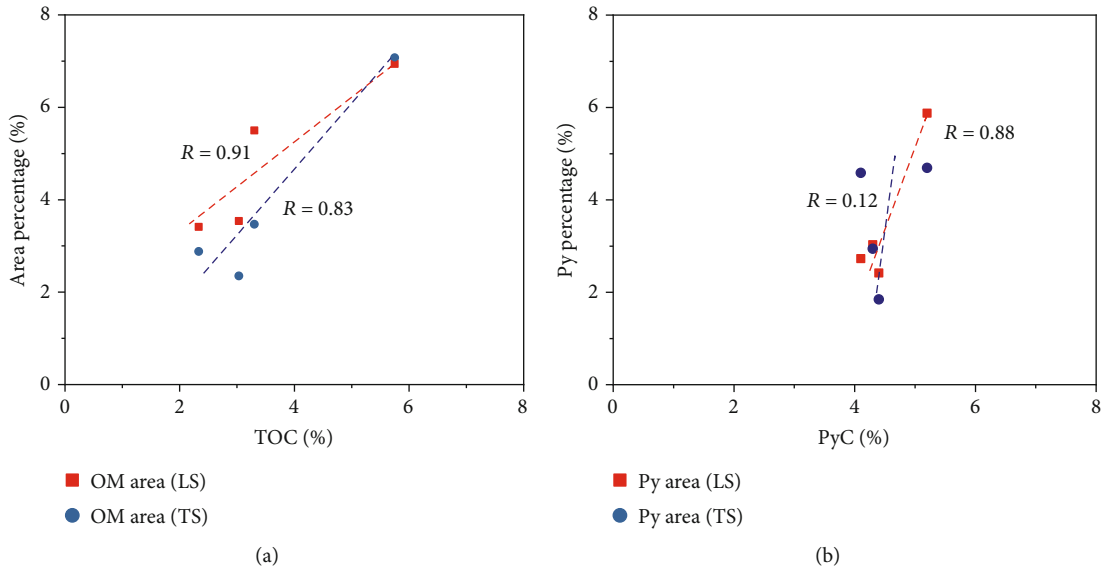

Figure 9: Area percentage of the grains in each image. (a) OM grains. (b) Py stands for pyrite grains. PyC stands for pyrite content.

The tendency of the OM grains orientation among the four samples seems counterintuitive cause it shows obvious differences in SEM images, especially for OM grains with large AR in sample BY and JY. However, due to the inner fractures or embedded inorganic mineral particles, many banded OM grains with obvious directionality may be identified as several individual particles during the binarization and segmentation, and this effect may be prominent in sample JY11and JY45 due to the embedded inorganic particles in OM grains. As Figure 10(c) shows, OM grains in sample JY11 and JY45 get similar AR with sample BY, while the banded OM grains get much larger AR in the SEM images, suggesting the calculated AR of the OM grains after segmentation is much smaller than that in SEM images. OM grains in LS of sample YY still get much larger AR after segmentation, because OM grains in sample YY are much lathy and very few inorganic particles are embedded.

As many banded OM grains are identified as several individual particles, the quantity of the segmented OM grains is much larger than we perceptually observed from SEM images. The number of OM grains identified by software ranges from 100 to 500 (Figure 10(d)), and the average number in sample JY11 is even larger than that of sample BY, which is counterintuitive to the SEM image observation. As Figure 10(b) shows, the SDA of sample JY45 is similar to sample BY, but OM grains in sample JY45 exhibit more definite directionality than sample BY in SEM images. The discrepancy may be the result of the disintegration of the banded grains, as the increment in grain quantity may heighten the dispersibility of the OM orientation and weaken the difference induced by banded OM grains. Moreover, the disintegration of the banded grains also decreases the AR of the grains, which may further weaken their directionality.

However, the holistic directional differences of the OM grains exhibited in LS and TS can still be fully embodied by the SDA. As shown in Figure 10(b), there are more OM grains arranged parallelly to bedding direction in LS of the samples, especially for sample YY. While in TS, the OM grains in four samples exhibit similar dispersions in their orientation and thus get very familiar SDA, which means the directivity of the OM grains in shale mainly exhibits in the LS of the formation, and this may be one of the reasons why some researchers regard shale as a transversely isotropic medium.

The image analyses indicate that many OM grains in shale are directionally arranged and are subparallel to the bedding section. However, the orientation degree of the OM grains varies significantly among different samples. In the four samples studied herein, OM grains in samples collected from C-7 formation exhibit the strongest directional alignment, and most OM grains are parallel to the bedding section. The alignment of OM grains in LMX shale samples collected from the Fuling area also exhibits strong directionality, while the directionality of the OM grains in LMX samples collected from Baojing is the weakest. Additionally, most OM grains in LMX shale that exhibited directional alignment are derived from graptolite.

4.3. Factors Affecting the Directionality of the OM Grains. According to the cross plots shown in Figure 11, OM grains in shale samples with higher clay content, TOC, and lower thermal maturity may exhibit more definite directionality in their orientation. As previously discussed, the major clay minerals of the shale samples herein are illite and illite/smectite mixed-layers, and both minerals get layered structure and of rich intergranular fractures. Additionally, they are usually subparallel to bedding sections, and, thus, they are commonly regarded as one of the vital factors affecting the anisotropy of shale.

Though clay minerals are usually treated as "soft" minerals in shale, recent AFM and nanoindentation studies have proved that OM grains are the softest component in shale [22, 23], and thus OM grains may be the first components to be squeezed and out of shape during the sedimentation.

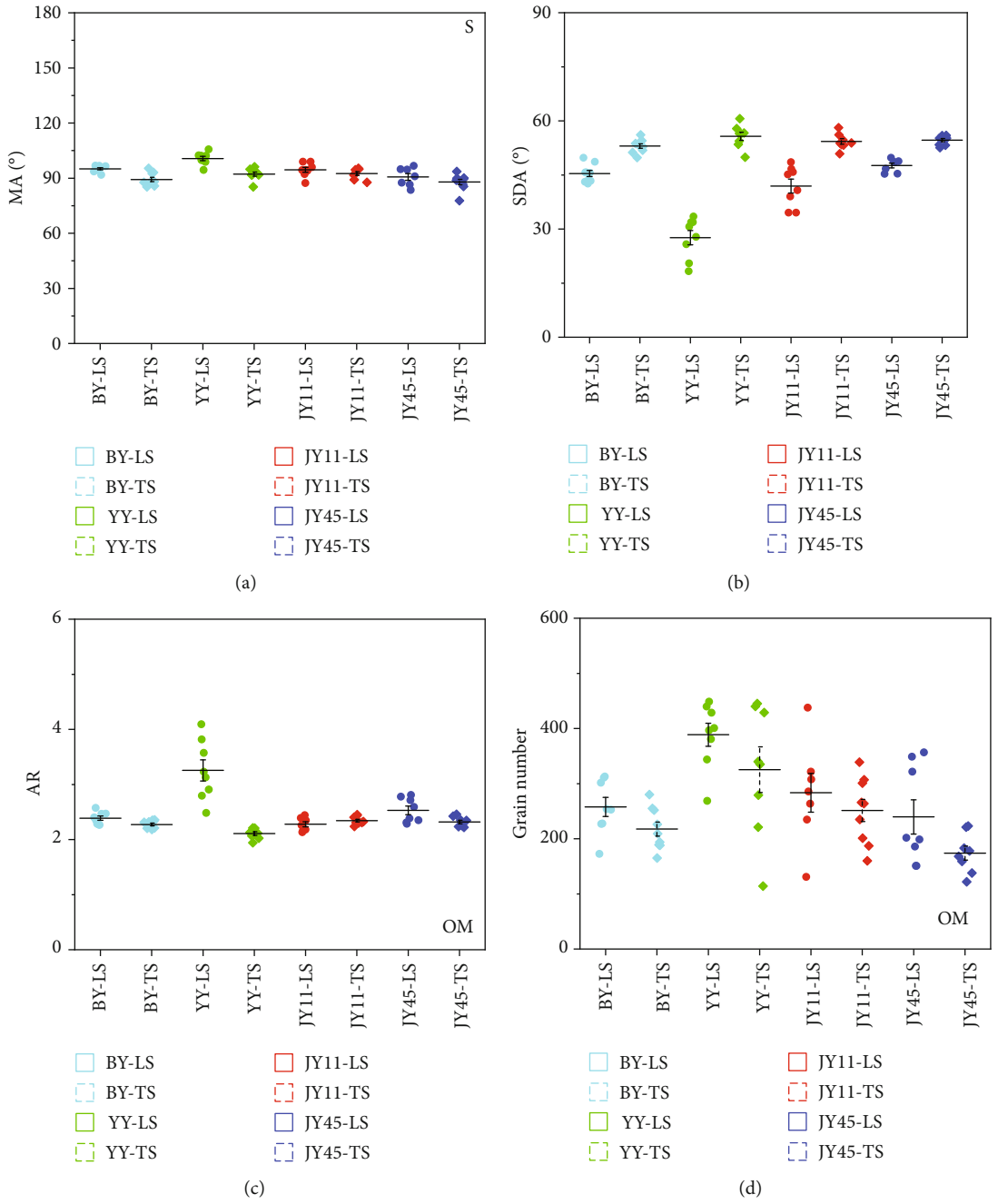

Figure 10: Statistical information of the OM grains in the four samples. (a) MA of OM grains in each image. (b) SDA of the OM grains angle in each image. (c) Average AR of the OM grains in each image. (d) OM grain numbers in each image.

They may be directly squeezed into strips by those layered clay minerals or be pushed into the fractures inner these layered clay minerals by other hard minerals, and both will increase the directionality of the OM grains. As samples from the C-7 Formation get the highest clay content and their OM grains are mainly derived from planktonic algae and lower hydrobiont [43], both types of OM get much weaker inherent structural anisotropy than graptolite. With the compaction of layered structure clay minerals, these OM grains are more likely to be deposited as banded grains. Therefore, the squeezing of the laminar clay minerals may be the dominant mechanism leading to the strong directionality of the OM grains in samples from C-7, and samples that contain more clay minerals tend to exhibit stronger directionality in the OM orientation. In comparison, banded OM grains in samples collected from LMX are mainly derived from graptolite remains. Due to its biogenetic texture, its directional orientation may be controlled by other mechanisms.

As Figure 12 shows, the inorganic mineral particles in shale samples from LMX (Figures 12(a) and 12(b)) are much larger than the sample from C-7(Figure 12(c)), and their average size is around 20~30 μm. While the average

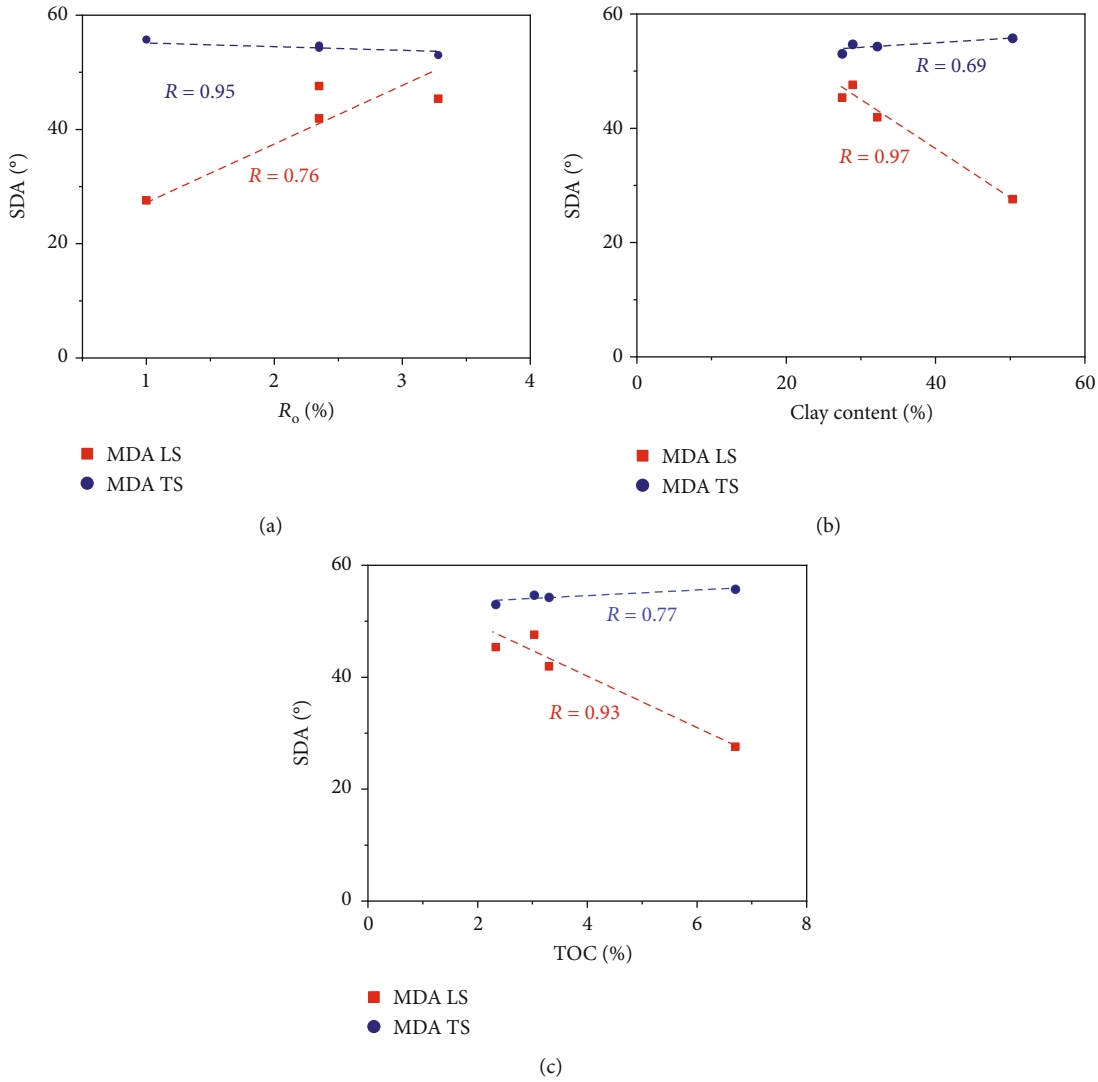

Figure 11: (a) Relationships between R_o and SDA. (b) Relationships between clay content and SDA. (c) Relationships between TOC and SDA.

grain size in sample YY is smaller than 10 μm and the largest grain is OM particles. The sedimental source mainly controls the grain size, and it may be the factor affecting the morphology of the OM edges. The sizes of the clay and mica particles in samples from LMX are similar to the adjacent OM grains, and these clay and mica grains usually get smooth edges. Thus, the adjoining OM grains may get similar smooth edges as the clay and mica particles after the squeezing.

While OM grains in sample YY border a mass of rugged small-sized clay or other inorganic mineral particles, the shape of the rugged inorganic particles may stamp on the OM grains after compaction, and, thus, jaggier edges are formed in these OM grains. With part of the jaggier edges been polished, these banded OM grains may exhibit as flocculent OM grains in TS of the samples, while the flocculent OM grains in samples from LMX may derive from the real amorphous OM grains.

The stress conditions may also affect the arrangement of the grains. Most clay or micas particles in LMX samples are subparallel to the banded OM grains in LS (Figures 12(a) and 12(b)), and some clay sheets are thicker than the adjacent OM grains in samples from LMX (Figure 12(c)). If the main extrusion force is orthometric to grains depositional plane, the adjacent OM grains will be squeezed into strips by these clay minerals, and this phenomenon is widely observed in samples JY45 and JY11. While in sample BY, the structure of clay minerals is more jumbly due to their much smaller size (Figure 12(e)). Though their inner sheet structures can still be observed, their orientation is more changeable, and, thus, the adjoining OM grains are of various shapes, suggesting these OM and clay grains may be squeezed from multiple directions. While most clay grains in sample YY are well parallel and OM grains are embedded in these directionally arrayed clay sheet clusters (Figure 12(f)), which implies the main extrusion force in sample YY is also perpendicular to the depositional plane. The difference in clay and OM arrangement in sample BY may mainly be caused by the tectonism, because sample BY is collected from the bottom of a syncline, where the horizontal stress is much higher. The high horizontal stress may disorganize the preformed laminated structure and deform the shape of the laminar OM

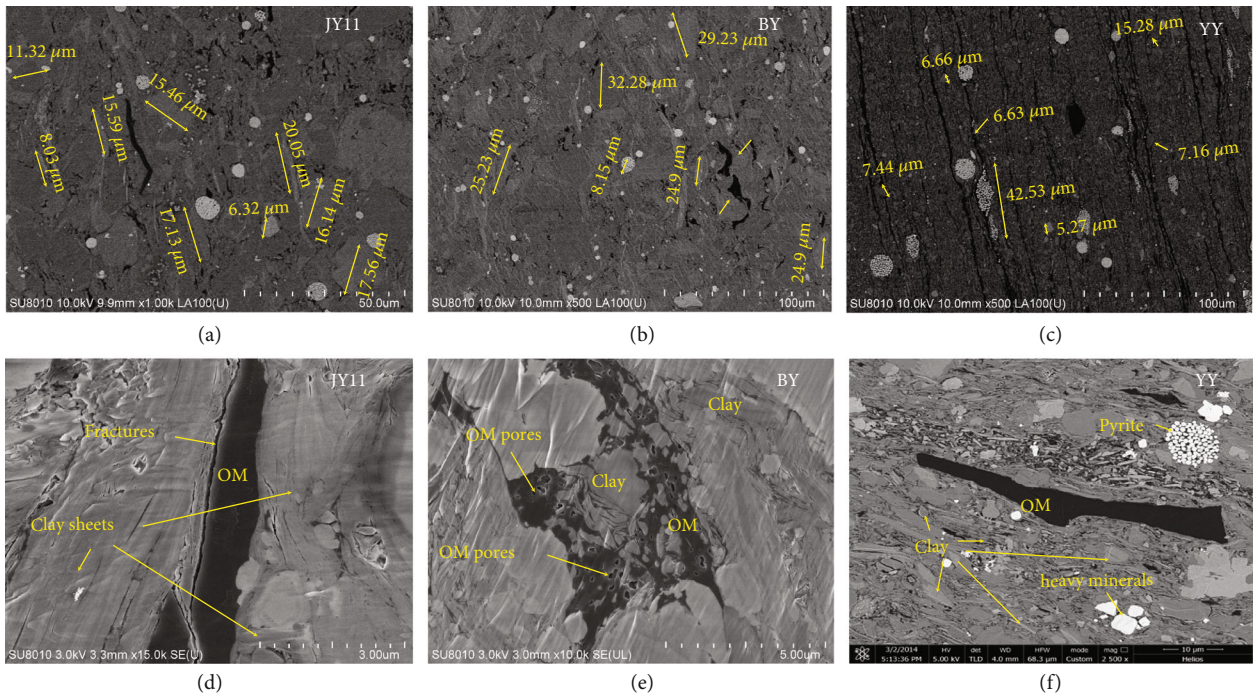

Figure 12: Size and morphology of the mineral grains in LS and TS of the four samples.

and clay grains. While sample YY, JY11, and JY45 are all collected from formations with the flatter structure and weaker horizontal stress. Thus, the laminated structure of the clay and OM grains is better preserved.

As shown in Figure 11(a), thermal maturity is closely related to the directional arrangement of OM in shale. Due to the sedimental environment differences, OM in sample YY is mainly derived from planktonic algae and lower hydrobiont. While in LMX samples, OM is mainly originated from planktons (graptolite, radiolarian, etc.), microbes, and algae [44]. Among these OM grains, algae are relatively harder to be preserved during the thermal maturation, and their structural features are almost indistinguishable when R_o is larger than 1.0 [45]. These OM may entirely or partially decompose as the thermal maturity goes higher. Consequently, their inner pressure will increase and organic pores may appear, and both will alter the geometry and arrangement of the OM grains. Thus, OM grains in samples with higher thermal maturity usually exhibit weaker directionality in their orientation.

However, the development of organic pores varies among different OM types. Bitumen usually gets well-developed pores, and algal fragments may have angular pores, while graptolites are relatively tight and usually have few or no pores [22]. Sample YY gets the lowest thermal maturity, and organic pores are less developed among most OM grains. Thus, the structure and shape of the OM grains in sample YY are well preserved. OM grains that exhibited directionality in samples from LMX mostly are derived from graptolite, though the thermal maturity of sample JY is much higher than sample YY, graptolite in LMX can be well preserved due to the componential difference [36], and the structure of graptolite is lamellate. Thus, graptolite may contribute more to the OM directionality than other types of OM in LMX. However, the maturation may still decompose or reshape other types of OM, which may decrease the total amount of the directionally distributed OM grains and thus weaken the holistic directionality. Considering graptolites account for 20 to 93% of the dispersed OM in LMX [33], the intrinsic biological structural characteristics of graptolites may be the dominating factor leading to the directional array of OM grains in samples from LMX. Nevertheless, complex tectonic movement may disorganize all the previously formed directional arrangement of OM or other grains in both marine and terrestrial shale. Thus, the influence factors of OM grains orientation in shale are diversified and complicated, and the orientation of OM grains in shales should be specifically analyzed, and OM grains should not be treated as an equally distributed medium in shale.

5. Conclusions

(1) OM grains in shale are not evenly distributed in isotropic medium, and their directional orientation is pervasive in both marine and terrestrial shale. Most OM grains in LS of the formation tend to array subparallel to the bedding section, while their orientation in TS is nearly random

(2) The orientation degree of the OM grains and their controlling factor differ a lot among different shales. OM grains in shale samples from C-7 and LMX in the Fuling area exhibit strong directional orientation, while OM grains in samples from LMX in the Baojing area exhibit much weaker directionality. The orientation of the OM grains in shale is closely related to the

clay content, thermal maturity, content and type of the OM, and tectonism of the formation

(3) The directional orientation of OM grains in samples from C-7 is mainly dominated by their high TOC and clay content, and the compaction of the directional arrayed platy clay minerals in the primary mechanism. The biogenetic texture of graptolite is the dominating mechanism leading to the directional alignment of the OM grains in LMX shale in the Fuling area. The weak directional arrangement of the OM grains in LMX shale in Baojing area may be mainly caused by the horizontal squeezing induced by the syncline structure

Data Availability

The data used to support the findings of this study are available from the corresponding author upon request.

Conflicts of Interest

The authors declare that they have no conflicts of interest.

Acknowledgments

The authors are thankful to two anonymous reviewers for their insightful comments and suggestions that have significantly improved the manuscript. This work was supported by the Chinese National Science and Technology Major Project (2017ZX05039-004) and Strategic Cooperation Technology Projects of CNPC and CUPB (ZLZX2020-01). The authors would like to thank Jianghan Oilfield Company for providing part of the core samples.

References

[1] C. Bobko and F. J. Ulm, "The nano-mechanical morphology of shale," *Mechanics of Materials*, vol. 40, no. 4-5, pp. 318–337, 2008.

[2] S. Zamiran, S. Rafieepour, and M. Ostadhassan, "A geomechanical study of Bakken formation considering the anisotropic behavior of shale layers," *Journal of Petroleum Science and Engineering*, vol. 165, pp. 567–574, 2018.

[3] D. B. Shaw and C. E. Weaver, "The mineralogical composition of shales," *Journal of Sedimentary Research*, vol. 35, no. 1, pp. 213–222, 1965.

[4] S. Zhou, N. Yang, and H. Wang, "Investigation of methane adsorption mechanism on Longmaxi shale by combining the micropore filling and monolayer coverage theories," *Advances in Geo-Energy Research*, vol. 2, no. 3, pp. 269–281, 2018.

[5] T. Zhang, G. S. Ellis, S. C. Ruppel, K. Milliken, and R. Yang, "Effect of organic-matter type and thermal maturity on methane adsorption in shale-gas systems," *Organic Geochemistry*, vol. 47, pp. 120–131, 2012.

[6] Z. Guo, X.-Y. Li, and C. Liu, "Anisotropy parameters estimate and rock physics analysis for the Barnett Shale," *Journal of Geophysics and Engineering*, vol. 11, no. 6, Article ID 065006, 2014.

[7] X. Li, X. Lei, and Q. Li, "Response of velocity anisotropy of shale under isotropic and anisotropic stress fields," *Rock Mechanics and Rock Engineering*, vol. 51, no. 3, pp. 695–711, 2018.

[8] W. Zhang and Q. Wang, "Permeability anisotropy and gas slippage of shales from the Sichuan Basin in South China," *International Journal of Coal Geology*, vol. 194, pp. 22–32, 2018.

[9] Y. Wan, Z. Pan, S. Tang, L. D. Connell, D. D. Down, and M. Camilleri, "An experimental investigation of diffusivity and porosity anisotropy of a Chinese gas shale," *Journal of Natural Gas Science and Engineering*, vol. 23, pp. 70–79, 2015.

[10] M. Mokhtari and A. N. Tutuncu, "Characterization of anisotropy in the permeability of organic-rich shales," *Journal of Petroleum Science and Engineering*, vol. 133, pp. 496–506, 2015.

[11] H. Zhu, Y. Ju, C. Huang, F. Chen, B. Chen, and K. Yu, "Microcosmic gas adsorption mechanism on clay-organic nanocomposites in a marine shale," *Energy*, vol. 197, article 117256, 2020.

[12] C. M. Sayers and L. D. den Boer, "Shale anisotropy and the elastic anisotropy of clay minerals," in *2014 SEG Annual Meeting*, Society of Exploration Geophysicists, 2014.

[13] D. N. Dewhurst and A. F. Siggins, "Impact of fabric, microcracks and stress field on shale anisotropy," *Geophysical Journal International*, vol. 165, no. 1, pp. 135–148, 2006.

[14] O. Kwon, A. K. Kronenberg, A. F. Gangi, B. Johnson, and B. E. Herbert, "Permeability of illite-bearing shale: 1. Anisotropy and effects of clay content and loading," *Journal of Geophysical Research: Solid Earth*, vol. 109, no. B10, 2004.

[15] B. E. Hornby, L. M. Schwartz, and J. A. Hudson, "Anisotropic effective-medium modeling of the elastic properties of shales," *Geophysics*, vol. 59, no. 10, pp. 1570–1583, 1994.

[16] G. Panizza and C. L. Ravazzoli, "An efficient rock-physics workflow for modeling and inversion in anisotropic organic-shales," *Journal of Petroleum Science and Engineering*, vol. 180, pp. 1101–1111, 2019.

[17] K. Liu, M. Ostadhassan, T. Gentzis, H. Carvajal-Ortiz, and B. Bubach, "Characterization of geochemical properties and microstructures of the Bakken shale in North Dakota," *International Journal of Coal Geology*, vol. 190, pp. 84–98, 2018.

[18] P. Cosenza, D. Prêt, A. L. Fauchille, and S. Hedan, "Representative elementary area of shale at the mesoscopic scale," *International Journal of Coal Geology*, vol. 216, p. 103316, 2019.

[19] S. Lohr, E. T. Baruch, P. A. Hall, and M. J. Kennedy, "Is organic pore development in gas shales influenced by the primary porosity and structure of thermally immature organic matter?," *Organic Geochemistry*, vol. 87, pp. 119–132, 2015.

[20] F. P. Wang and R. M. Reed, "Pore networks and fluid flow in gas shales," in *Paper presented at the SPE Annual Technical Conference and Exhibition*, New Orleans, Louisiana, October 2009.

[21] Q. Luo, G. Fariborz, N. Zhong et al., "Graptolites as fossil geothermometers and source material of hydrocarbons: an overview of four decades of progress," *Earth-Science Reviews*, vol. 200, p. 103000, 2020.

[22] W. Zhang, W. Hu, T. Borjigin, and F. Zhu, "Pore characteristics of different organic matter in black shale: a case study of the Wufeng-Longmaxi formation in the Southeast Sichuan Basin, China," *Marine and Petroleum Geology*, vol. 111, pp. 33–43, 2020.

[23] Y. Liu, Y. Xiong, and Y. Li, "Effect of thermal maturation on chemical structure and nanomechanical properties of solid bitumen," *Marine and Petroleum Geology*, vol. 92, pp. 780–793, 2018.

[24] S. Emmanuel, M. Eliyahu, R. J. Day-Stirrat, R. Hofmann, and C. I. Macaulay, "Impact of thermal maturation on nano-scale elastic properties of organic matter in shales," *Marine and Petroleum Geology*, vol. 70, pp. 175–184, 2016.

[25] K. Liu, M. Ostadhassan, and B. Bubach, "Applications of nano-indentation methods to estimate nanoscale mechanical properties of shale reservoir rocks," *Journal of Natural Gas Science and Engineering*, vol. 35, pp. 1310–1319, 2016.

[26] W. Li and A. Sakhaee-Pour, "Macroscale Young's moduli of shale based on nanoindentations," *Petrophysics*, vol. 57, no. 6, pp. 597–603, 2016.

[27] A. Gabova, E. Chekhonin, Y. Popov et al., "Experimental investigation of thermal expansion of organic-rich shales," *International Journal of Rock Mechanics and Mining Sciences*, vol. 132, p. 104398, 2020.

[28] C. Yang, J. Zhang, X. Tang et al., "Comparative study on micro-pore structure of marine, terrestrial, and transitional shales in key areas, China," *International Journal of Coal Geology*, vol. 171, pp. 76–92, 2017.

[29] C. Cui, Z. Dong, and D. Wu, "Rock mechanics study and fracability evaluation for Longmaxi formation of Baojing block in Hunan Province," *Natural Gas Geoscience*, vol. 30, no. 5, pp. 626–634, 2019.

[30] J. Cui, R. Zhu, S. Li, Y. Qi, X. Shi, and Z. Mao, "Development patterns of source rocks in the depression lake basin and its influence on oil accumulation: case study of the Chang 7 member of the Triassic Yanchang formation, Ordos Basin, China," *Natural Gas Geoscience*, vol. 4, no. 4, pp. 191–204, 2019.

[31] W. Ji, F. Hao, Y. Song, J. Tian, M. Meng, and H. Huang, "Organic geochemical and mineralogical characterization of the lower Silurian Longmaxi shale in the southeastern Chongqing area of China: implications for organic matter accumulation," *International Journal of Coal Geology*, vol. 220, p. 103412, 2020.

[32] Z. Qiu, C. Zou, X. Li et al., "Discussion on the contribution of graptolite to organic enrichment and gas shale reservoir: a case study of the Wufeng-Longmaxi shales in South China," *Journal of Natural Gas Geoscience*, vol. 3, no. 3, pp. 147–156, 2018.

[33] Q. Luo, N. Zhong, N. Dai, and W. Zhang, "Graptolite-derived organic matter in the Wufeng-Longmaxi Formations (Upper Ordovician-Lower Silurian) of southeastern Chongqing, China: implications for gas shale evaluation," *International Journal of Coal Geology*, vol. 153, pp. 87–98, 2016.

[34] T. Saif, Q. Lin, A. R. Butcher, B. Bijeljic, and M. J. Blunt, "Multi-scale multi-dimensional microstructure imaging of oil shale pyrolysis using X-ray micro-tomography, automated ultra-high resolution SEM, MAPS mineralogy and FIB-SEM," *Applied Energy*, vol. 202, pp. 628–647, 2017.

[35] I. Arganda Carreras, V. Kaynig, C. Rueden et al., "Trainable Weka segmentation: a machine learning tool for microscopy pixel classification," *Bioinformatics*, vol. 33, no. 15, pp. 2424–2426, 2017.

[36] Y. Ma, N. Zhong, L. Cheng et al., "Pore structure of the graptolite-derived OM in the Longmaxi shale, southeastern upper Yangtze region, China," *Marine and Petroleum Geology*, vol. 72, pp. 1–11, 2016.

[37] C. Yan, Z. Jin, J. Zhao, W. Du, and Q. Liu, "Influence of sedimentary environment on organic matter enrichment in shale: a case study of the Wufeng and Longmaxi formations of the Sichuan Basin, China," *Marine and Petroleum Geology*, vol. 92, pp. 880–894, 2018.

[38] R. Morga and M. Kamińska, "The chemical composition of graptolite periderm in the gas shales from the Baltic basin of Poland," *International Journal of Coal Geology*, vol. 199, pp. 10–18, 2018.

[39] R. Morga and M. Pawlyta, "Microstructure of graptolite periderm in Silurian gas shales of northern Poland," *International Journal of Coal Geology*, vol. 189, pp. 1–7, 2018.

[40] C. M. Link, R. M. Bustin, and F. Goodarzi, "Petrology of graptolites and their utility as indices of thermal maturity in lower Paleozoic strata in northern Yukon, Canada," *International Journal of Coal Geology*, vol. 15, no. 2, pp. 113–135, 1990.

[41] M. E. Curtis, B. J. Cardott, C. H. Sondergeld, and C. S. Rai, "Development of organic porosity in the Woodford shale with increasing thermal maturity," *International Journal of Coal Geology*, vol. 103, pp. 26–31, 2012.

[42] H. Nie, Z. Jin, and J. Zhang, "Characteristics of three organic matter pore types in the Wufeng-Longmaxi shale of the Sichuan Basin, Southwest China," *Scientific Reports*, vol. 8, no. 1, pp. 1–11, 2018.

[43] X. Z. Wang, J. C. Zhang, J. Z. Cao et al., "A preliminary discussion on evaluation of continental shale gas resources: a case study of Chang 7 of Mesozoic Yanchang formation in Zhiluo-Xiasiwan area of Yanchang," *Earth Science Frontiers*, vol. 19, no. 2, pp. 192–197, 2012.

[44] C. Liang, Z. Jiang, C. Zhang, L. Guo, Y. Yang, and J. Li, "The shale characteristics and shale gas exploration prospects of the lower Silurian Longmaxi shale, Sichuan Basin, South China," *Journal of Natural Gas Science and Engineering*, vol. 21, pp. 636–648, 2014.

[45] J. Cai, X. Zhu, J. Zhang, M. Song, and Y. Wang, "Heterogeneities of organic matter and its occurrence forms in mudrocks: evidence from comparisons of palynofacies," *Marine and Petroleum Geology*, vol. 111, pp. 21–32, 2020.